

**ESTIMATION OF HARMONICS, INTERHARMONICS AND SUB-HARMONICS IN  
MOTOR DRIVE SYSTEMS**

by

**Robert John Kerestes**

B.S. in Electrical Engineering, University of Pittsburgh, 2010

M.S. in Electrical Engineering, University of Pittsburgh, 2011

Submitted to the Graduate Faculty of  
Swanson School of Engineering in partial fulfillment  
of the requirements for the degree of  
Doctor of Philosophy

University of Pittsburgh

2014

UNIVERSITY OF PITTSBURGH  
SWANSON SCHOOL OF ENGINEERING

This dissertation was presented

by

Robert John Kerestes

It was defended on

November 15<sup>th</sup>, 2013

and approved by

Zhi-Hong Mao, Ph.D., Associate Professor, Electrical and Computer Engineering

Thomas McDermott, Ph.D., Assistant Professor, Electrical and Computer Engineering

Chengtao Wen, Ph.D., Emerson Process Management

Dissertation Director: Gregory F. Reed, Ph.D., Associate Professor, Electrical and Computer

Engineering

Copyright © by Robert J. Kerestes

2014

# **ESTIMATION OF HARMONICS, INTERHARMONICS AND SUB-HARMONICS IN MOTOR DRIVE SYSTEMS**

Robert Kerestes, Ph.D.

University of Pittsburgh, 2014

Harmonic analysis in power systems is a challenge that is always evolving due to a constantly changing power grid. Advances in power electronics have led to the installation of many new non-linear power loads, such as power converters, arc furnaces and motor drive systems, which in turn change the existing infrastructure and inject new types of harmonics. This study analyzes a static Kramer drive system for its harmonic behavior. The system is broken down component-by-component and analyzed. The analysis includes classical harmonics of integer multiple of the fundamental frequency as well as sub-harmonics and interharmonics. This paper shows that there are significant harmonic issues in a static Kramer drive that are likely to be present in similar drive systems.

Due to the unknown frequencies at which interharmonics and sub-harmonics arise it is difficult to estimate the magnitude and phase of these harmonics. It is proposed that state estimation techniques such as digital filtering coupled with windowing techniques can be used to properly pinpoint the frequency components, magnitudes and phases of harmonics, interharmonics and sub-harmonics in the motor drive systems. Once identified, the harmonics, interharmonics and sub-harmonics can be eliminated by means of passive filtering or self-tuning active filtering.

The optimal methods of estimation of harmonics, interharmonics and sub-harmonics will be both developed analytically and through the means of simulation with the use of CAD tools

such as PSCAD and MATLAB. The development of the optimal techniques for estimation of harmonics, interharmonics and sub-harmonics for that static Kramer drive will aid in estimation of harmonics, interharmonics and sub-harmonics in similar motor drive systems.

## TABLE OF CONTENTS

<b>PREFACE.....</b>	<b>XII</b>
<b>1.0 INTRODUCTION.....</b>	<b>1</b>
<b>1.1 BACKGROUND .....</b>	<b>1</b>
<b>1.2 STATEMENT OF THE PROBLEM.....</b>	<b>2</b>
<b>1.3 THESIS LAYOUT.....</b>	<b>3</b>
<b>2.0 LITERATURE REVIEW.....</b>	<b>5</b>
<b>2.1 THE POWER SYSTEM HARMONIC .....</b>	<b>5</b>
<b>2.1.1 Harmonics of Integer Multiple of the Fundamental .....</b>	<b>6</b>
<b>2.1.2 Interharmonics.....</b>	<b>10</b>
<b>2.1.3 Sub-harmonics .....</b>	<b>13</b>
<b>2.1.4 Harmonic Elimination.....</b>	<b>15</b>
<b>2.1.4.1 Passive Harmonic Filters.....</b>	<b>15</b>
<b>2.1.4.2 Active Harmonic Filters .....</b>	<b>17</b>
<b>2.2 ESTIMATION TECHNIQUES.....</b>	<b>19</b>
<b>2.2.1 The Method of Least-Squares .....</b>	<b>20</b>
<b>2.2.2 The Method of Weighted Least-Squares Estimation .....</b>	<b>22</b>
<b>2.2.3 The Kalman Filter .....</b>	<b>23</b>
<b>3.0 TEST SYSTEM.....</b>	<b>25</b>

<b>4.0</b>	<b>HARMONIC ANALYSIS .....</b>	<b>27</b>
<b>4.1</b>	<b>FOURIER ANALYSIS OF THE STATIC KRAMER COMPONENTS.....</b>	<b>27</b>
<b>4.1.1</b>	<b>Fourier analysis of the Doubly Fed Induction Motor .....</b>	<b>27</b>
<b>4.1.2</b>	<b>Fourier analysis of the Uncontrolled Six-Bridge Rectifier .....</b>	<b>33</b>
<b>4.1.3</b>	<b>Fourier analysis of the Three-Phase Inverter .....</b>	<b>40</b>
<b>4.1.4</b>	<b>Fourier analysis of a Three-phase Transformer System .....</b>	<b>46</b>
<b>5.0</b>	<b>SYSTEM SIMULATION .....</b>	<b>50</b>
<b>5.1</b>	<b>CONSTRUCTION OF THE STATIC KRAMER DRIVE SYSTEM IN SIMPOWERSYSTEMS.....</b>	<b>50</b>
<b>5.2</b>	<b>PERFORMACE OF THE STATIC KRAMER DRIVE CIRCUIT .....</b>	<b>54</b>
<b>5.3</b>	<b>EXPORTING SIGNALS INTO MATLAB.....</b>	<b>56</b>
<b>6.0</b>	<b>HARMONIC ESTIMATION TECHNIQUEUS .....</b>	<b>62</b>
<b>6.1.1</b>	<b>Estimation through the Use of a Band Pass Filter.....</b>	<b>62</b>
<b>6.1.1.1</b>	<b>Analytical Development for Band Pass Filter .....</b>	<b>63</b>
<b>6.1.1.2</b>	<b>Simulation Results of the Band Pass Filter.....</b>	<b>66</b>
<b>6.1.2</b>	<b>Estimation through the Use of a Low Pass Filter .....</b>	<b>67</b>
<b>6.1.2.1</b>	<b>Analytical Development of the Low Pass Filter .....</b>	<b>68</b>
<b>6.1.2.2</b>	<b>Simulation Result of the Low Pass Filter.....</b>	<b>70</b>
<b>6.1.3</b>	<b>Estimation through the a Phase Shifting Low Pass Filter .....</b>	<b>72</b>
<b>6.1.3.1</b>	<b>Analytical Development of the Phase Shifting Low Pass Filter.....</b>	<b>72</b>
<b>6.1.3.2</b>	<b>Analysis of the Phase Shifting Low Pass Filter’s Tuning Parameters</b>	<b>75</b>
<b>6.1.3.3</b>	<b>Simulation of the Phase Shifting Low Pass Filter .....</b>	<b>78</b>

<b>7.0</b>	<b>DISCUSSION .....</b>	<b>81</b>
<b>8.0</b>	<b>CONCLUSION.....</b>	<b>82</b>
	<b>BIBLIOGRAPHY.....</b>	<b>84</b>

## LIST OF FIGURES

Figure 2-1: Power Systems Signal Showing the Fundamental, Some Odd Harmonics and their Combined Waveform [8]. .....	6
Figure 2-2: Waveform with Harmonic and Interharmonic Components [3]. .....	11
Figure 2-3: Typical Cycloconverter Current Spectrum (60 Hz Power System) [3]. .....	13
Figure 2-4: Illustration of Sub-harmonic Frequencies in the Frequency Spectrum of a Typical Cycloconverter. ....	14
Figure 2-5: (a) Single-Tuned Shunt Filter; (b) Second-Order Damped Shunt Filter.....	16
Figure 2-6: A Series Connected Active Filter with an AC Source and a Non-Linear Load.....	17
Figure 2-7: A Shunt Connected Active Filter with an AC Source and a Non-Linear Load.....	18
Figure 2-8: (a) Distorted Load Current; (b) Effect of Compensation by Means of a Shunt Connected Active Filter [27]. .....	19
Figure 3-1: Static Kramer Drive System [35].....	25
Figure 4-1: PSCAD Schematic of a Wound-Rotor Induction Motor .....	29
Figure 4-2: Speed, Electrical Torque and Mechanical Torque vs. Time During the Transient Period of Simulation .....	30
Figure 4-3: Stead State Motor Stator and Rotor Currents after Transient Effects have Terminated .....	31
Figure 4-4: Single Sided Frequency Spectrum of Stator and Rotor Current .....	32
Figure 4-5: top: Three-phase Alternating Current Waveform; bottom: Resulting Rectified Direct Current Waveform [40].....	33
Figure 4-6: PSCAD Circuit of a Three-Phase Rectifier.....	34
Figure 4-7: Illustration of the First 0.3 Seconds of the Three-Phase Rectifier Circuit.....	35

Figure 4-8: DC Current Ripple in Three-Phase Rectifier Circuit .....	37
Figure 4-9: Single Sided Frequency Spectrum of the Three-Phase Rectifier Circuit.....	38
Figure 4-10: Illustration of Sub-Harmonics and Interharmonics for the Three-Phase Rectifier Circuit .....	39
Figure 4-11: Three-phase Inverter PSCAD Schematic.....	40
Figure 4-12: Transistor Firing Sequence and Resultant Line to Line Voltage Waveform .....	41
Figure 4-13: Inverted Three-Phase Current .....	42
Figure 4-14: Inverted Phase A Current.....	43
Figure 4-15: Single Sided Frequency Spectrum of Three Phase Inverter .....	44
Figure 4-16: Single Sided Frequency Spectrum of Three-Phase Inverter with Interharmonic Components .....	45
Figure 4-17: Wiring Diagram for a Wye-Delta Grounded Transformer .....	46
Figure 4-18: PSCAD Schematic Diagram for Three Phase Transformer.....	47
Figure 4-19: Primary and Secondary Current for the Wye-Delta Transformer.....	47
Figure 4-20: Single Sided Frequency Spectrum for Primary Current (a); Single Sided Frequency Spectrum for Secondary Current (b).....	48
Figure 5-1 SimPowerSystems Model of Static Kramer Drive System.....	51
Figure 5-2: Current Drawn by the Stabilizing Resistive Load .....	52
Figure 5-3: Voltage and Current Waveforms Measured from the Source.....	54
Figure 5-4: Rectified Direct Current Waveform with Strong Harmonics Present.....	55
Figure 5-5: Output Waveform Sent Back to the System Load .....	55
Figure 5-6: Phase-to-Phase Voltage of the System Output .....	56
Figure 5-7: Capturing Voltage Signals Using the Simout Simulink Block.....	57
Figure 5-8: Text File Containing Input and Output Voltage Readings .....	58
Figure 5-9: Voltage from the System's Source (top); Voltage from the System's Output (bottom) .....	59
Figure 5-10: Fast Fourier Transform of the Input and Output Signal for the System .....	60

Figure 5-11: Fast Fourier Transform of the Input and Output Signal from a Larger Scale of Frequencies .....	61
Figure 6-1: Block Diagram Representation of the Band Pass Filter.....	63
Figure 6-2: Frequency Response of Analytic Band Pass Filter .....	65
Figure 6-3: Magnitude Response of Analytic Band Pass Filter.....	65
Figure 6-4: Frequency response for Least-Squares Band-Pass Filter.....	66
Figure 6-5: Voltage Wave with Band Pass Filter Applied .....	67
Figure 6-6: Block Diagram Representation of the Low Pass Filter.....	68
Figure 6-7: Frequency Response of Analytic Low Pass Filter .....	69
Figure 6-8: Frequency Response for Low Pass Equiripple Filter.....	71
Figure 6-9: Voltage Wave with Low Pass Filter Applied.....	71
Figure 6-10: Block Diagram Representation of the Phase Shifting Low Pass Filter .....	72
Figure 6-11: Magnitude Response of Phase Shifting Low Pass Filter with Respect to Varying $\alpha$ .....	76
Figure 6-12: Phase Response of Phase Shifting Low Pass Filter with Respect to Varying $\alpha$ .....	77
Figure 6-13: Phase Response of Phase Shifting Low Pass Filter with Respect to Varying $\beta$ .....	77
Figure 6-14: Voltage Wave with Low Pass and All Pass Filter Applied.....	79
Figure 6-15: Fourier Analysis for the Low Pass and All Pass Filtered Signal .....	80

## **PREFACE**

I dedicate this work to my wonderful girlfriend Amanda Buerkle and my son Noah. I could not have done it without them. I would also like to thank Dr. Reed, Dr. Kusic, Dr. Mao, Dr. McDermott and Dr. Wen for serving on my Ph.D. dissertation committee and providing their priceless guidance.

## **1.0 INTRODUCTION**

One of the greatest challenges that exist in the power systems of today is how to deal with voltage and current harmonics. This problem has been around nearly as long as the existence of alternating current power systems and continues to be a challenge for power systems engineers [1]. To this day, harmonics in power systems still continue to be a problem because the electrical grid is always changing. There is an increasing number of non-linear loads being introduced to the grid such as power converters, arc furnaces and controlled motor drives, all which cause power systems harmonics [2].

### **1.1 BACKGROUND**

Motor drive systems have several unwanted harmonic components to their current waveforms due to the makeup of these systems. Motor drive systems usually are made up of an induction machine which has two different frequencies associated with it and hence is likely to cause current harmonics. Also, motor drive systems contain power electronic devices such as rectifiers and inverters. As was stated earlier power electronics devices such as rectifiers and inverters are known sources of harmonic distortion.

The problem of harmonics in power systems has been investigated for quite some time. However, the problem of interharmonics and sub-harmonics has not been studied as long [3-5].

This should be clear from the last IEEE standard on power systems harmonics [4] which does not give a thorough treatment of sub-harmonics and interharmonics. The study of interharmonics is still evolving today, and that goes especially for specific components in power systems which are known to generate interharmonics.

## **1.2 STATEMENT OF THE PROBLEM**

It is quite common for motor drive systems to contain harmonics, sub-harmonics and interharmonics throughout the makeup of the system. Many of these drive systems have been thoroughly analyzed in the past for their harmonic components alone but not for their interharmonic and sub-harmonic components [6]. A motor drive system was analyzed for its harmonics, sub-harmonics and interharmonics through the use of Fourier analysis to gain insight on the problem areas of the drive system. This analysis was used to develop signal processing techniques such as parameter estimation through filtering to accurately yield the magnitude and phase of signals in motor drive systems. Three different methods of filtering, simple band-pass filtering, simple low-pass filtering and phase shifting low-pass filtering were used and compared for their strengths and weaknesses to determine the most optimal method of filtering for this particular problem. The development of adequate estimation through these signal processing techniques will lead to active or passive filtering, chosen based on some economic analysis, so that the harm to the system due to harmonic distortion can either be removed or at least reduced. This work will lead into further harmonic, interharmonic and sub-harmonic analysis, estimation and elimination in other drive systems, arc furnaces and similar non-linear loads.

### 1.3 THESIS LAYOUT

Chapter 2.0 provides a review of the literature that was used for this study. Power systems harmonics were studied as classical harmonics, interharmonics and sub-harmonics. Methods of eliminating harmonics through passive and active filtering are covered in this chapter. Some common techniques of estimating harmonics in power systems are reviewed and discussed in this chapter as well.

Chapter 3.0 gives a detailed technical representation of the test system that was used for this study. The system that was chosen was the Static Kramer Drive System due to its abundance of harmonic generating components.

Chapter 4.0 provides harmonic analysis on each of the systems components to pinpoint exactly where the harmonic distortion in the system may arise from. This analysis was simulation based using of combination of the CAD packages PSCAD and MATLAB. Each component is analyzed using classical Fourier analysis.

Chapter 5.0 provides the simulation of the system as a whole including the construction of the system in MATLAB's SimPowerSystems, analysis of the performance of the system and the method of transferring signals from different MATLAB components.

Chapter 6.0 describes the methods of estimation that were used on the Static Kramer Drive System. These methods of estimation were analytically derived and compared versus their respective simulation results. The method of phase shifting low pass filtering couple with tuning methods to achieve optimal estimation is derived and analyzed in detail both in the Laplace domain and the time domain. The effectiveness of tuning parameters and their ability to produce then most optimal method of estimation is described in this chapter as well.

Chapter 7.0 provides a brief discussion of this study which compares the test system used in this study with similar systems and elaborates on how the study can be used for similar motor drive systems.

Chapter 8.0 provides some concluding remarks about the study including possible future work and projects that can be produced as a result of this study.

## **2.0 LITERATURE REVIEW**

This chapter describes harmonics in power systems as well as the methods of harmonic state estimation and adaptive filtering that currently exists. These methods are elaborated by describing their pros and cons as well as their usefulness in further solving this problem.

### **2.1 THE POWER SYSTEM HARMONIC**

Harmonics in power systems are voltages and currents which have frequencies other than the fundamental frequency. For the most part, power systems harmonics have a frequency which is an integer multiple of the fundamental frequency, however that is not always the case [1, 7-9]. Power signals can also contain components which have frequencies which are non-integer multiples of the fundamental frequency. These components are referred to as inter-harmonics. Similarly to the inter-harmonics contained in power systems are sub-harmonics. Sub-harmonics are components of a power signal which have a frequency that is a fraction of the fundamental frequency. This section gives a treatment of power systems harmonics of integer multiples of the fundamental, interharmonics and sub-harmonics including their causes and the effect that they have on components of the power system.

### 2.1.1 Harmonics of Integer Multiple of the Fundamental

The most common harmonics in power systems are those which are of an integer multiple of the fundamental frequency [8]. In 1822 J.B.J. Fourier proposed in [10], that any function that is continuously repetitive on an interval  $T$  can be represented as the summation of a D.C. component, a fundamental sinusoid component and a series of higher-order sinusoids at frequencies which are multiples of the fundamental frequencies. These harmonics usually have a magnitude which is much smaller than the magnitude of the fundamental and are usually shifted in phase from the fundamental. An example of a power system signal with harmonic components can be seen in Figure 2-1.

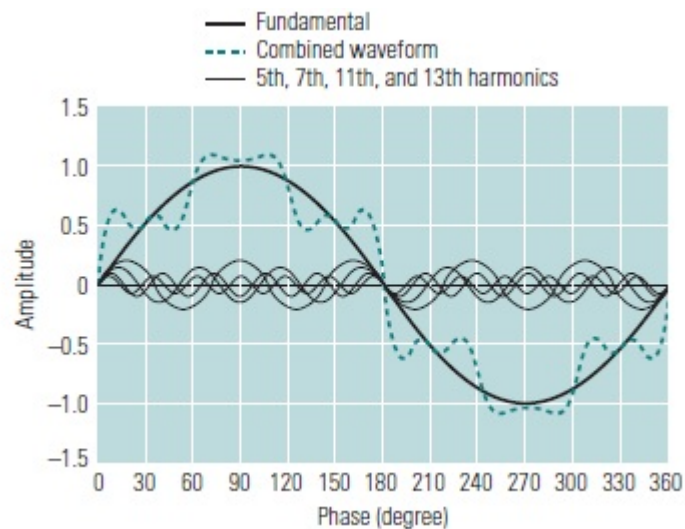


**Figure 2-1.** Power Systems Signal Showing the Fundamental, Some Odd Harmonics and their Combined Waveform [8]

Figure 2-1 illustrates a power system signal with the 5<sup>th</sup>, 7<sup>th</sup>, 11<sup>th</sup> and 13<sup>th</sup> harmonic components, as well as the fundamental component. Likewise Figure 2-1 illustrates the

combination of all of these components and the distorting effect that they have on the fundamental waveform.

A periodic power systems signal can be mathematically represented as given in [10] by the following equation

$$x(t) = a_0 + \sum_{n=1}^{\infty} a_n \cos(n\omega_1 t) + b_n \sin(n\omega_1 t) \quad (2.1)$$

where  $\omega_1$  is the signal's fundamental frequency given in radians. Each component of equation (2.1) can be calculated by equations (2.2)-(2.4).

$$a_0 = \frac{1}{2\pi} \int_{-\pi}^{\pi} x(\omega t) d(\omega t) \quad (2.2)$$

$$a_n = \frac{1}{\pi} \int_{-\pi}^{\pi} x(\omega t) \cos(n\omega t) d(\omega t) \quad (2.3)$$

$$b_n = \frac{1}{\pi} \int_{-\pi}^{\pi} x(\omega t) \sin(n\omega t) d(\omega t) \quad (2.4)$$

Equation (2.1) can be manipulated according to the methods given in [1] and represented in a more practical representation as given in equation (2.5).

$$x(t) = d_0 + \sum_{n=1}^{\infty} d_n \sin(n\omega_1 t + \psi_n) \quad (2.5)$$

where

$$d_n = \sqrt{a_n^2 + b_n^2} \quad (2.6)$$

$$\psi_n = \tan^{-1} \left( \frac{a_n}{b_n} \right) \quad (2.7)$$

Equation (2.5) is more practical because it clearly gives a magnitude and phase shift of each of the harmonic components. A second way that that equation (2.1) can be manipulated is according to the methods given in [1, 11, 12] yielding the complex representation of equation (2.1) given in equation (2.8).

$$x(t) = \sum_{n=-\infty}^{\infty} c_n e^{jn\omega_1 t} \quad (2.8)$$

where

$$c_n = \frac{1}{2}(a_n - jb_n) \quad (2.9)$$

$$c_{-n} = c_n^* \quad (2.10)$$

$$c_0 = a_0 \quad (2.11)$$

Each individual  $c_n$  term can individually be calculated using equations (2.12) and (2.13).

$$c_n = \frac{1}{\pi} \int_{-\pi}^{\pi} x(\omega t) e^{-jn\omega t} d(\omega t) \quad (2.12)$$

$$c_0 = \frac{1}{2\pi} \int_{-\pi}^{\pi} x(\omega t) d(\omega t) \quad (2.13)$$

Power systems signals are primarily measurements of voltage and current [13, 14]. Hence, it is helpful to implement equation (2.5) in terms of voltage and current. Using trigonometric identities, equation (2.5) can take the form of voltage and current in equations (2.14) and (2.15) as given in [15].

$$v(t) = V_0 + \frac{1}{\sqrt{2}} \sum_{n=1}^{\infty} v_{n(rms)} \cos(n\omega_1 t + \alpha_n) \quad (2.14)$$

$$i(t) = I_0 + \frac{1}{\sqrt{2}} \sum_{n=1}^{\infty} i_{n(rms)} \cos(n\omega_1 t + \beta_n) \quad (2.15)$$

where  $V_0$  and  $I_0$  are the D.C. components of the voltage and current signals,  $v_{n(rms)}$  and  $i_{n(rms)}$  are the root mean squared values of the  $n^{th}$  voltage and current harmonic and  $\alpha_n$  and  $\beta_n$  are the respective phases of for the  $n^{th}$  voltage and current harmonic.

An important quantity which gives an overall measure of the “distortion” of the signal is referred to as the total harmonic distortion (THD) [4, 15]. The equations for total harmonic distortion of voltage (THD<sub>v</sub>) and total harmonic distortion of current (THD<sub>i</sub>) are given in equations (2.16) and (2.17).

$$\text{THD}_v = \frac{\sqrt{\sum_{n=2}^{\infty} (V_n^2)}}{V_1} \quad (2.16)$$

$$\text{THD}_i = \frac{\sqrt{\sum_{n=2}^{\infty} (I_n^2)}}{I_1} \quad (2.17)$$

Some last and final quantities that may be of interest when performing a study on power systems harmonics are the real, reactive and apparent power of the D.C. component, the fundamental and each subsequent harmonic [1, 13-15]. The real, reactive and apparent powers for the quantities aforementioned are given in equations (2.18) and (2.19).

$$P_n = V_{n(rms)} I_{n(rms)} \cos(\alpha_n - \beta_n) \quad (2.18)$$

$$Q_n = V_{n(rms)} I_{n(rms)} \sin(\alpha_n - \beta_n) \quad (2.19)$$

$$S_n = V_{n(rms)} I_{n(rms)} \quad (2.20)$$

where  $P_n$  represents the real power for the  $n^{th}$  harmonic,  $Q_n$  represents the reactive power for the  $n^{th}$  harmonic and  $S_n$  represents the apparent power for the  $n^{th}$  harmonic. Moreover, the total real, total reactive and total apparent powers are given in equations (2.21)-(2.23).

$$P_{\text{total}} = \sum_{n=0}^{\infty} P_n \quad (2.21)$$

$$Q_{\text{total}} = \sum_{n=1}^{\infty} Q_n \quad (2.22)$$

$$S_{\text{total}} = \sum_{n=1}^{\infty} S_n \quad (2.23)$$

It should be noted that in the treatment of power systems harmonics in this section, all equations consider harmonics ranging from zero to infinity. For power systems studies the highest harmonic  $n_{\text{max}}$  is sufficient in a range of two to twenty-five but most standards use fifty [1, 2, 9, 15]. All equations in practice will have an upper limit of  $n_{\text{max}}$  rather than infinity and this value will be clearly stated in this study.

### 2.1.2 Interharmonics

Harmonics with frequency of integer multiple of the fundamental frequency, or traditional harmonics one could say, have been studied extensively since nearly the dawn of ac systems. As the power systems grid continually changes, however, new phenomena related to traditional power systems harmonics are being introduced. As intermodulation between the fundamental and the harmonic components of a system occur, a component with a frequency of a non-integer multiple can occur [3]. These components are referred to as interharmonics. A precise definition of interharmonics is given in [3, 16] as:

“Between the harmonics of the power frequency voltage and current, further frequencies can be observed which are not an integer (multiple) of the fundamental. They can appear as discrete frequencies or as a wide band spectrum.”

Moreover the interharmonic frequency component of a power systems signal can be defined mathematically as was done in [3] as

$$\omega \neq n\omega_1 \text{ where } n \text{ is an integer } > 0 \quad (2.24)$$

Figure 2-2 illustrates a waveform that has both harmonic and interharmonic components. In a power systems waveform such as a voltage or current waveform one would not expect the effects of the harmonic and interharmonic components to be as drastic as in Figure 2-2, however, this figure is a good illustration of how a waveform can be distorted.

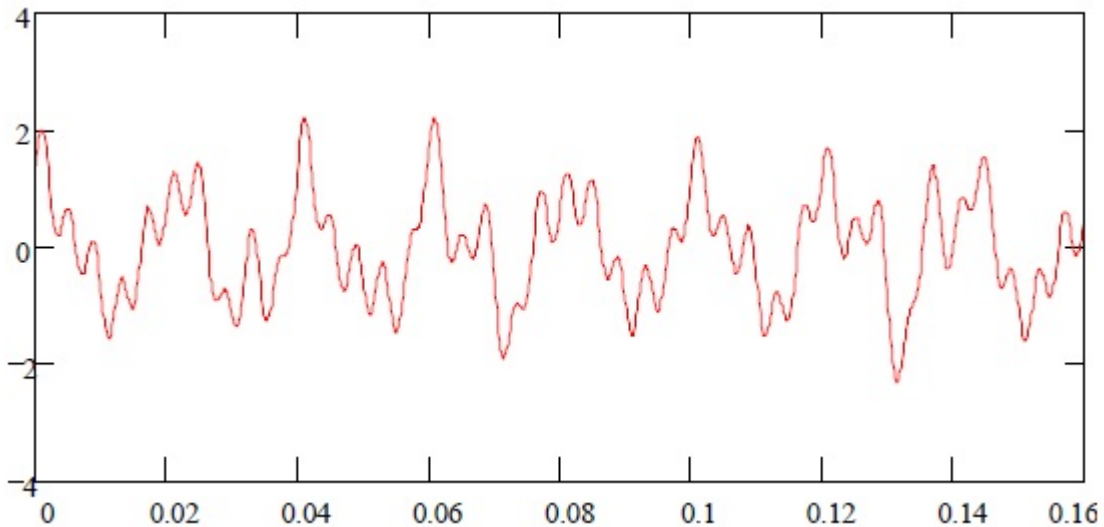


**Figure 2-2.** Waveform with Harmonic and Interharmonic Components [3]

Interharmonics are rapidly becoming a problem in power systems due to the drastic increase in interharmonic inducing loads. These loads include but are not limited to [3, 16, 17]

- Static frequency converters
- Cycloconverters
- Sub-synchronous converter cascades
- Induction motors
- Arc furnaces
- HVDC schemes
- Large DC link drives to synchronous or induction motors

The chief source of interharmonic generation is the cycloconverter [3, 18, 19]. However, with the exponentially increasing number of power electronic devices in power systems, several interharmonic sources are of interest. Figure 2-3 illustrates the frequency spectrum for the current of a typical cycloconverter in a 60 Hz system. It can be seen from Figure 2-3 that there are significant current magnitudes at frequencies other than the fundamental 60 Hz component or integer multiples of the fundamental. Also, it should be noted that there are magnitudes at frequencies below the fundamental 60 Hz component. These are a special type of interharmonic called a sub-harmonic. Sub-harmonics will be given a brief treatment in the following section.

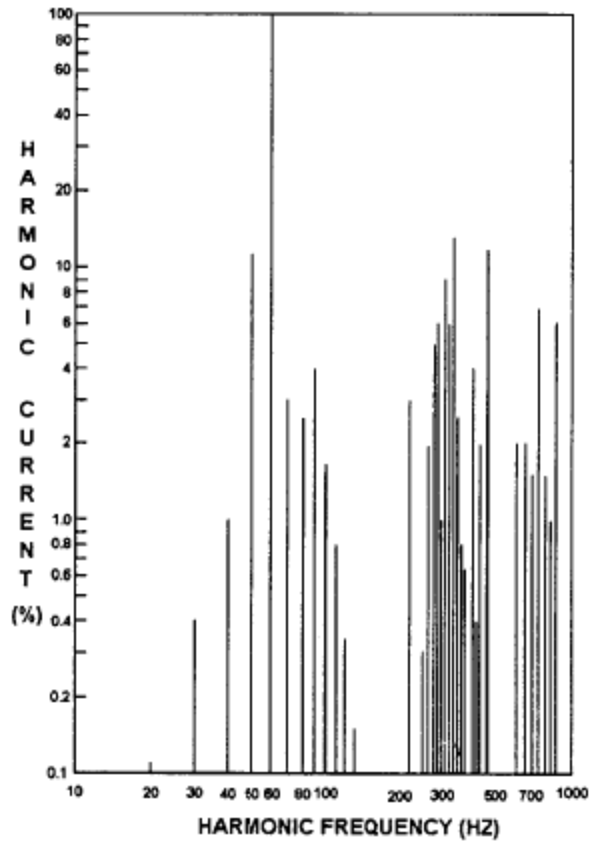


Figure 2-3. Typical Cycloconverter Current Spectrum (60 Hz Power System) [3]

### 2.1.3 Sub-harmonics

As was described in the previous section, sub-harmonics have a frequency which is a non-integer multiple of the fundamental frequency and their frequency is less than the fundamental frequency. A sub-harmonic frequency is described mathematically in equation (2.25).

$$f > 0 \quad \text{and} \quad f < f_1 \quad (2.25)$$

These components can be seen clearly from the frequency spectrum of the cycloconverter illustrated in Figure 2-3. This is illustrated in Figure 2-4.

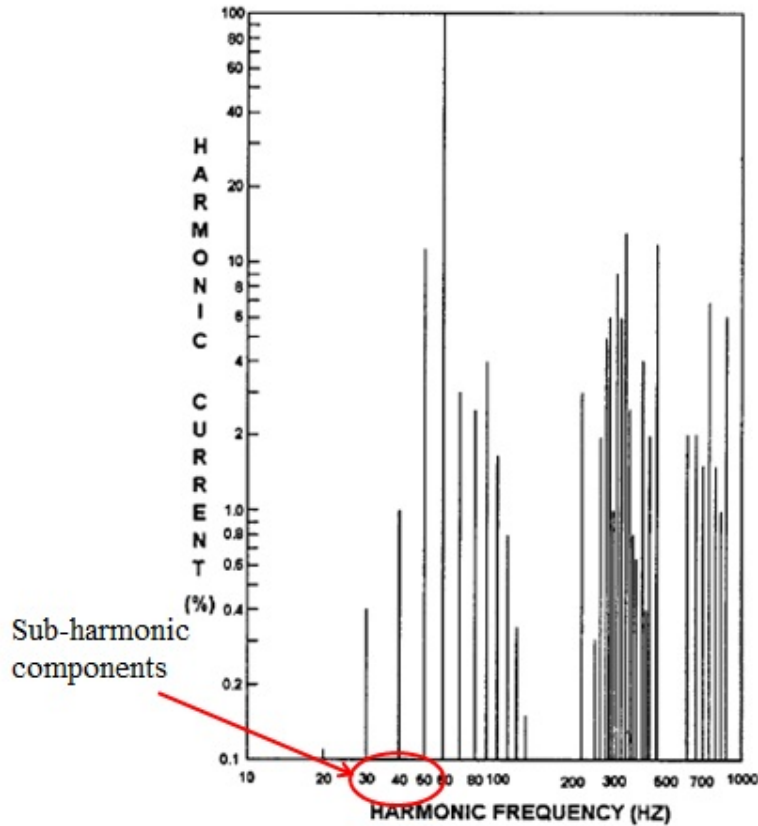


**Figure 2-4.** Illustration of Sub-harmonic Frequencies in the Frequency Spectrum of a Typical Cycloconverter

As expected, because sub-harmonics are a specific type of interharmonic, sub-harmonics are caused by many of the same sources as the interharmonics with a frequency greater than the fundamental frequency. These sources include cycloconverters, arc furnaces, automated spot welders and so on [5, 18, 20]. Also, it should be noted that systems which contain more than one power converter cascaded together such as vehicular systems i.e. electric and hybrid electric vehicles, sea vehicles, aircraft and space stations [21]. While this subset of interharmonics is only a class of interharmonics and affect power quality in much the same way, they should be noted as a class of their own for further analysis.

## **2.1.4 Harmonic Elimination**

This section gives a brief explanation of some well-defined methods of eliminating harmonic components in power systems. Of course, the optimal solution for the elimination of trouble causing harmonics is to design a system that does not contain them. This is often the approach taken on D.C. systems which have cascaded converters, however this is not always feasible. When this design approach is not feasible, other means of harmonic elimination must be implemented.

### **2.1.4.1 Passive Harmonic Filters**

The simplest method for the elimination of harmonics in power systems is the method of filtering by means of a passive filter. For the most part we only want to use a clean fundamental component of a power systems signal. Therefore, it only makes sense to design a filter which attenuates the undesirable harmonic, interharmonic and sub-harmonic components of a power systems signal. This approach is straight forward and easy to implement however it has its drawbacks, mainly being cost and ineffectiveness to filter interharmonics and sub-harmonics [1]. Passive filters in power systems are commonly designed as second order shunt filters of one of two flavors. The first is a single tuned shunt filter which can be seen in Figure 2-5 (a). The second is a second-order damped shunt filter which can be seen in Figure 2-5 (b).

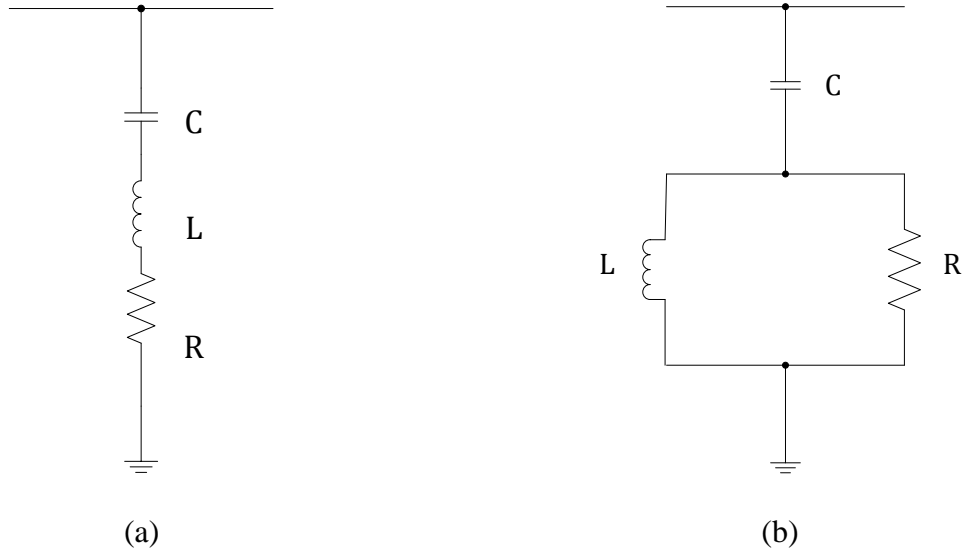


**Figure 2-5.** (a) Single-Tuned Shunt Filter; (b) Second-Order Damped Shunt Filter

Due to the fact that both of the aforementioned passive filters are of second order they both have a quality factor ( $Q$ ). The quality factor of a filter is a dimensionless value which describes how under-damped a second order filter is [22]. This relates to the transfer function of the special case of a low pass second order filter as would be used to passively filter power systems harmonics as given in equation (2.26).

$$H(s) = \frac{\omega_n^2}{s^2 + \frac{\omega_n}{Q}s + \omega_n^2} \quad (2.26)$$

Looking at the quality factor in the form of equation (2.26) puts it into perspective quite well. Using some basic knowledge of second order systems, as the  $Q$  becomes larger the system becomes less damped and conversely as  $Q$  becomes smaller the system becomes more damped. Generally the value of  $Q$  ranges from 0.5 to 500 [23].

Though passive filters are generally a straight forward method of eliminating harmonics in practice they have the drawbacks of design complexity, high cost, limited range of

effectiveness and the introduction of system resonance [1, 24]. For these reasons other means of harmonic elimination have been developed.

#### 2.1.4.2 Active Harmonic Filters

Due to some of the drawbacks of passive harmonic filtering that were previously mentioned active filters are designed and implemented. The concept of actively filtering power systems harmonics has been studied since the early 1970s shortly thereafter put into practice [25, 26]. One of the particular benefits of active filters over their passive counterpart is the ability to eliminate interharmonics and sub-harmonics.

The active filter works on a similar principal to reactive power compensation, but rather than compensating reactive power, unwanted harmonic current is compensated. There are two methods of active filtering, active filtering through a series connection and active filtering through a shunt connection. Figure 2-6 shows a circuit with a non-linear load and a series connected active filter.

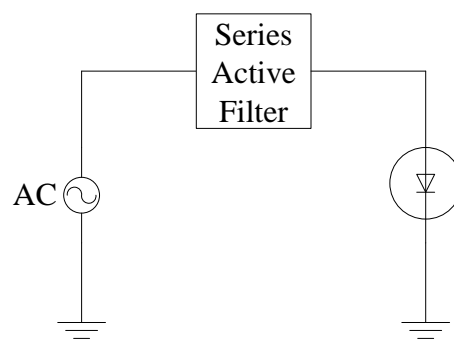


**Figure 2-6.** A Series Connected Active Filter with an AC Source and a Non-Linear Load

The second configuration for active filtering is illustrated in Figure 2-7. This figure shows the shunt connected active filter.

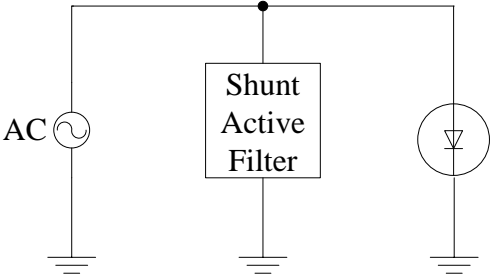


**Figure 2-7.** A Shunt Connected Active Filter with an AC Source and a Non-Linear Load

The topologies that are mentioned in Figure 2-6 and Figure 2-7 implement an active filter through means of power electronic devices. Many of the above topologies implement a passive filter combined with an active filter to allow the harmonic currents to circulate through the passive filter component. Figure 2-8 illustrates the effect of compensation effect of a shunt connected active filter.

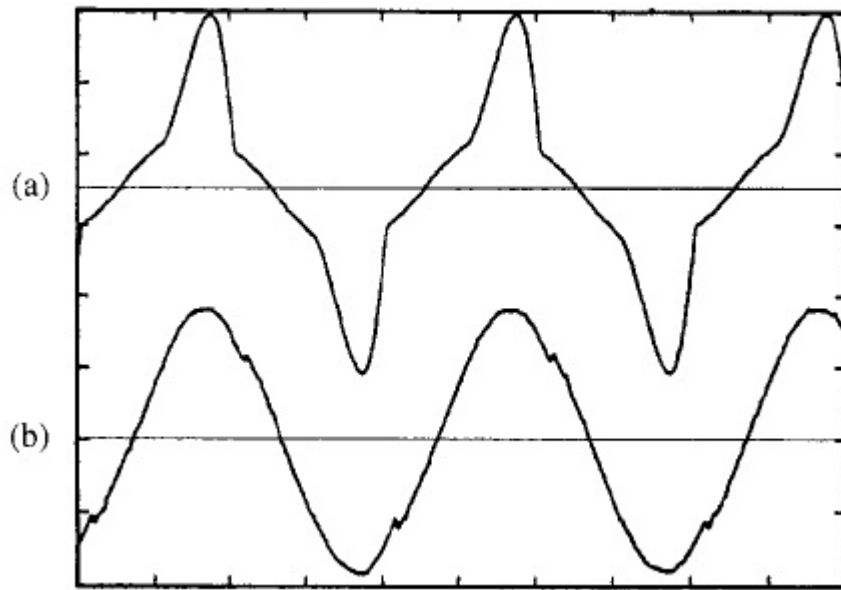


**Figure 2-8.** (a) Distorted Load Current; (b) Effect of Compensation by Means of a Shunt Connected Active Filter [27]

Although, active filtering has many benefits, it still has the downfall of being expensive due to its power electronic components. As the cost of inverters goes down with advancements in semiconductor technology, however, this should be less of a problem.

## 2.2 ESTIMATION TECHNIQUES

State feedback is used in power systems to provide stability, optimality and other performance standards as required by some specifications [28]. Ideally all of the state variables or all components of the state vector are available. However, often times in large power systems this is not the case. Often times one or more of these variables are not available or cannot be obtained practically because of accessibility or the high cost of measurement instrumentation [29]. If any of these variables is not available either the power flow solution or some other calculation for a

power systems network cannot be calculated or it will be so erroneous that it will be of no use [14]. In order to provide the missing state variables so that state feedback can be applied the technique of state estimation is used. State estimation refers to the technique of using available measurement to estimate missing data in some optimal way. The technique of state estimation was first implemented around the 1800s by Carl Friedrich Gauss [30]. Gauss had invented the technique of deterministic least-squares which was applied to an orbit measurement problem [31]. Many new techniques have developed since Gauss had formulated the method of deterministic least-squares. This section will give a summary of existing state estimation techniques.

### 2.2.1 The Method of Least-Squares

As was previously mentioned, the method of least-squares was first developed by Gauss for the use of astronomical studies. However, since then, this method has been used for many other areas which have a use for estimation [32].

To describe the method of least-squares we first must look at the linear observation equation.

$$\mathbf{z} = \mathbf{H}\mathbf{x} + \mathbf{v} \quad (2.27)$$

Equation 2.27 gives the linear observation equation of a system which requires state estimation. In this equation  $\mathbf{x}$  is the state vector which has dimension  $n$ ,  $\mathbf{H}$  is referred to as the observation matrix which has dimensions  $(k_I \times n)$ , where  $k_I \geq n$ ,  $\mathbf{v}$  is the error vector or the measurement noise vector of dimension  $k_I$  and  $\mathbf{z}$  is the measurement vector which also has dimension  $k_I$ . The goal is

to calculate an estimate of the state  $\mathbf{x}$  notated as  $\hat{\mathbf{x}}$ . Using this estimate the output of the system can be calculated using equation (2.28).

$$\hat{\mathbf{y}} = \mathbf{H}\hat{\mathbf{x}} \quad (2.28)$$

From equations (2.27) and (2.28) two terms can be defined. The term state residual is mathematically defined as given in equation (2.29)

$$\mathbf{e}_x = \mathbf{x} - \hat{\mathbf{x}} \quad (2.29)$$

And the term measurement residual is mathematically defined as given in equation (2.30)

$$\mathbf{e}_z = \mathbf{z} - \hat{\mathbf{y}} \quad (2.30)$$

Using the quadratic cost function for both the state residual as given in equation (2.31) and the measurement residual as given in equation (2.32) the least squares estimator can be developed.

$$\mathbf{J}(\mathbf{x}) = \frac{1}{2} \mathbf{e}_x^T \mathbf{e}_x \quad (2.30)$$

$$\mathbf{J}(\mathbf{z}) = \frac{1}{2} \mathbf{e}_z^T \mathbf{e}_z \quad (2.31)$$

Equations (2.30) and (2.31) can then be manipulated by the methods described in [28] to yield the least squares estimator. The least squares estimator is given in equation (2.32).

$$\hat{\mathbf{x}} = (\mathbf{H}^T \mathbf{H})^{-1} \mathbf{H}^T \mathbf{z} \quad (2.32)$$

This least-squares estimator yields an optimal estimate of the state in question by minimizing the sum of the squared errors.

## 2.2.2 The Method of Weighted Least-Squares Estimation

Because there are errors in measurements and not all of these errors are the same, one would conclude that all of these measurements should not hold equal weight when used to estimate a state of a system. For this reason the method of weighted least-squares estimation was developed [33].

The method of weighted least-squares estimation uses a weighting factor which weights good data (data without a lot of measurement error) more heavily than bad data (data with a lot of measurement error). This method is good for the parameter estimation of harmonic components of sinusoidal signals [34]. To illustrate this concept the technique of least-squares estimation which was discussed in Section 2.2.2 will be expanded upon.

The measurement residual for the  $k_{th}$  data point can be derived using equation (2.27), (2.28) and (2.30). This measurement residual is given in equation (2.33).

$$\mathbf{e}_{z_k} = \mathbf{H}_k \mathbf{e}_x + n_k \quad (2.33)$$

where  $\mathbf{H}_k$  is the  $k_{th}$  row on the matrix  $\mathbf{H}$ . For each  $k$  of equation (2.33), the equation can be normalized. Equation (2.34) shows this normalization

$$\mathbf{e}'_z = \mathbf{N}^{-1} \mathbf{e}_z \quad (2.34)$$

where

$$\mathbf{N} = \begin{bmatrix} v_1 & 0 & \cdots & 0 \\ 0 & v_2 & \cdots & 0 \\ \vdots & \vdots & \ddots & \vdots \\ 0 & 0 & 0 & v_{k_i} \end{bmatrix} \quad (2.35)$$

and

$$v_k = \mathbf{H}_k \mathbf{e}_x + n_k \quad (2.36)$$

Using equation (2.35) the diagonal weighting matrix can be developed. This matrix is given in equation (2.37)

$$\mathbf{S} = \mathbf{N}^T \mathbf{N} \quad (2.37)$$

Then using equation (2.37) the weighted least-squares estimator can be derived as was done in [28]. The weighted least-squares estimator is given in equation (2.38).

$$\hat{x} = (\mathbf{H}^T \mathbf{S}^{-1} \mathbf{H})^{-1} \mathbf{H}^T \mathbf{S}^{-1} \mathbf{z} \quad (2.38)$$

### 2.2.3 The Kalman Filter

Another method that has been used successfully for state estimation is the the Kalman filter. The Kalman filter uses a set of linear equations that are similar to the state space method of forming equations. Equation (2.39) gives the equation that governs the systems.

$$\mathbf{x}_k = \mathbf{A} \mathbf{x}_{k-1} + \mathbf{B} u_k + w_{k-1} \quad (2.39)$$

The object is to estimate the value of  $x \in \mathfrak{R}^n$  based on the previously mentioned equation and a measurement which is given in equation (2.40).

$$\mathbf{z}_k = \mathbf{H} \mathbf{x}_k + v_k \quad (2.40)$$

where  $w_k$  and  $v_k$  are the system noise and the measurement instrumentation noise respectively and  $\mathbf{H}$  is the observance matrix. In order for the Kalman filter to work correctly both the system noise and the measurement noise must be white normal Gaussian distributed. There are however, some techniques to alter the Kalman filter slightly so that it can be used with noise that is not

white normal Gaussian distributed. The Kalman gain matrix is given by the following equation. The derivation of this equation is quite extensive and can be seen in [28].

$$\mathbf{K}_k = \mathbf{P}_k(-)\mathbf{H}_k^T [\mathbf{H}_k \mathbf{P}_k(-)\mathbf{H}_k^T + \mathbf{R}_k]^{-1} \quad (2.41)$$

Where  $\mathbf{P}(-)$  is the covariance estimate extrapolation and the derivation for it can be found in [28]. Finally the estimator is given by equation (2.42)

$$\hat{\mathbf{x}}_k = \hat{\mathbf{x}}_k^- + \mathbf{K}_k (\mathbf{z}_k - \mathbf{H}_k \hat{\mathbf{x}}_k^-) \quad (2.42)$$

Where  $\hat{\mathbf{x}}_k^-$  replaces  $\mathbf{x}_{k-1}$ .

### 3.0 TEST SYSTEM

In order to analyze and estimate harmonics in a motor-drive system a test system would have to be created. The test system that was used was a static Kramer drive system. The static Kramer drive is composed of a three phase 60 Hz voltage source, a doubly fed induction motor, three phase rectifier, a three phase inverter and a transformer. The three phase 60 Hz source and the secondary end of the transformer are connected together so that excess power is fed back into the system. Figure 3-1 illustrates the topology for a static Kramer drive system.

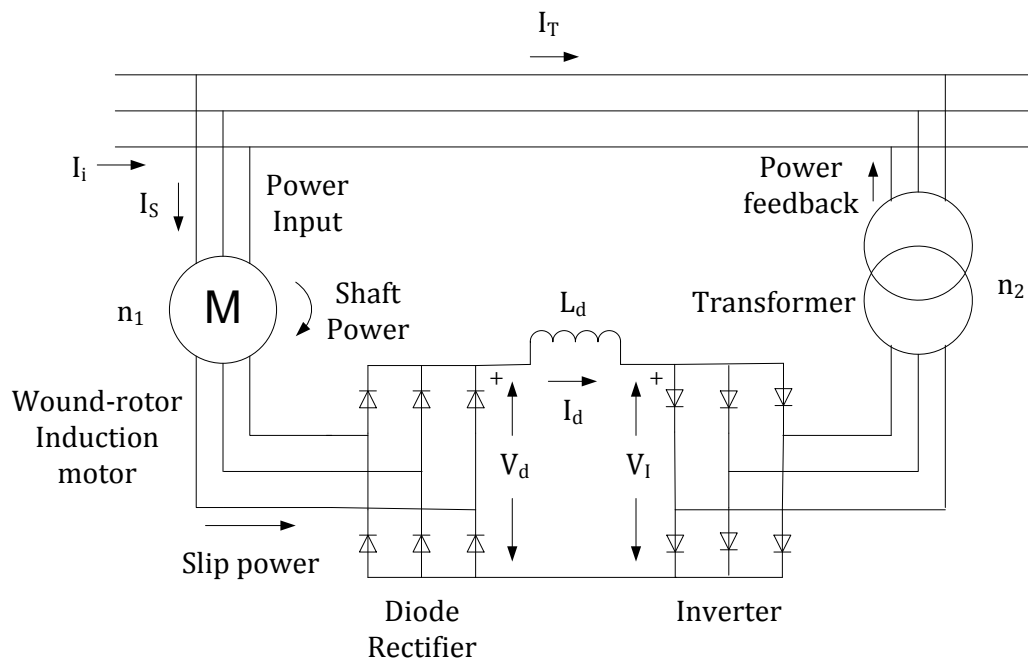


Figure 3-1. Static Kramer Drive System [35]

The induction motor of this system does not operate at exactly 60 Hz by the principle of an induction machine and it also has the slip frequency which is not at 60 Hz. For both of these reasons an induction motor generates interharmonics. As was stated in Chapter 2.0 sub-harmonics are often generated when cascading more than one power converter together. For this reason the static Kramer drive is a good candidate for sub-harmonics due to its cascaded rectifier-inverter combinations. Finally, integer multiple harmonics will be naturally generated by nearly every component of this system. The static Kramer drive system was chosen for this study because of the aforementioned harmonics, interharmonics and sub-harmonics that it generates.

## **4.0 HARMONIC ANALYSIS**

This section provides some of the preliminary results obtained in the proposal phase of the project based on simulation of the static Kramer drive system. The CAD software packages which are used to implement these simulations are PSCAD and MATLAB. The version of PSCAD that was used for the preliminary results is the student version which can analyze an electrical system of up to fifteen nodes. For this reason, the Kramer drive system was broken up into individual components. These components include the three-phase, 60 Hz voltage source which feeds the stator of the doubly fed induction motor, the uncontrolled six-bridge rectifier, the three phase inverter and a wye-delta transformer.

### **4.1 FOURIER ANALYSIS OF THE STATIC KRAMER COMPONENTS**

This section analyzes each component of the static Kramer drive system and provides some discussion on each component of the system.

#### **4.1.1 Fourier analysis of the Doubly Fed Induction Motor**

The induction motor is of interest in a study of interharmonics because as a system it contains more than just one frequency. For an induction motor, the upper limit of motor speed is the

mechanical equivalent of the electrical system frequency [38]. For example the upper limit of motor speed for a two pole machine would be 3600 rpm. This is referred to as the machine's synchronous speed. The difference in the actual speed of the motor's shaft, or the mechanical speed of the motor and the synchronous speed of the motor is defined as the slip speed of the motor. This relationship is given in equation 4.1.

$$n_{\text{slip}} = n_{\text{sync}} - n_{\text{mech}} \quad (4.1)$$

There is also the per-unit value (percentage value) of slip which is mathematically defined as

$$s = \frac{n_{\text{sync}} - n_{\text{mech}}}{n_{\text{sync}}} (\times 100\%) \quad (4.2)$$

An induction motor operates similarly to a transformer where the stator of the machine is referred to as the primary side of the machine and the rotor is referred to as the secondary side of the machine. An induction motor is also sometimes referred to as a rotary transformer [38]. What makes the induction motor different from a stationary transformer is that the primary side and secondary side have different frequencies. The primary side frequency will be the same frequency as the electrical input to the stator. The rotor however, will have a different frequency. The frequency of the machine's rotor can be mathematically defined as

$$f_{\text{rotor}} = sf_{\text{stator}} \quad (4.3)$$

Due to equation (4.3) it is clear that there will be more than one frequency present in any system that contains an induction motor. It should also be noted that if the rotor frequency is less than the stator frequency (which is the fundamental). For this reason the induction motor is likely to generate interharmonics and sub-harmonics in a system in which it is implemented.

This component of the static Kramer drive system was analyzed to get an understanding of its harmonic components. To do this a simulation of an induction motor was performed using PSCAD. The circuit simulated in PSCAD is shown in Figure 4-1.

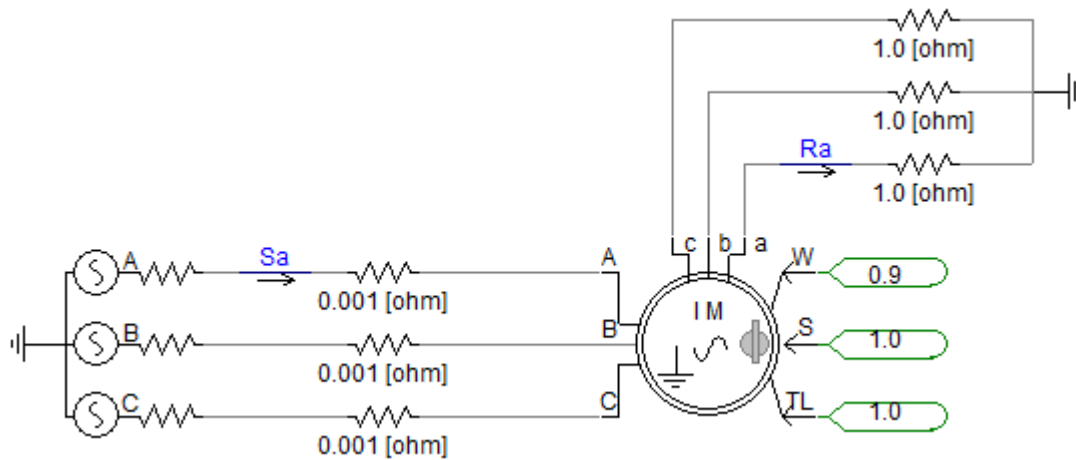


**Figure 4-1.** PSCAD Schematic of a Wound-Rotor Induction Motor

For this simulation the stator windings of the induction motor were supplied by a three-phase, 60 Hz, 460 V<sub>L-L</sub> source. The motor was rated at 460 V, 150 Hp. The motor ratings were gathered from a Baldor motor datasheet [39] so that the parameters were as realistic as possible. The default values of mechanical damping and angular moment of inertia were used. These values were 0.05 p.u. and 0.3 s respectively. The induction motor has two modes of operation; speed control and torque control. For this simulation the motor is run in speed control mode with a constant speed of 0.9 p.u. This yields a slip percentage of 10%. Using this information and equation (4.3) the rotor frequency can be calculated. This calculation is carried out in equation (4.4).

$$f_r = (0.1)(60) = 6 \text{ Hz} \quad (4.4)$$

This result can be verified through the simulation. The simulation was carried out for three seconds to ensure that any transient effects would die out. The only transient effects that are seen in this simulation are those of mechanical and electrical torque. The motor is operated in speed control mode with a constant speed so there are no speed transients. This behavior can be seen in Figure 4-2

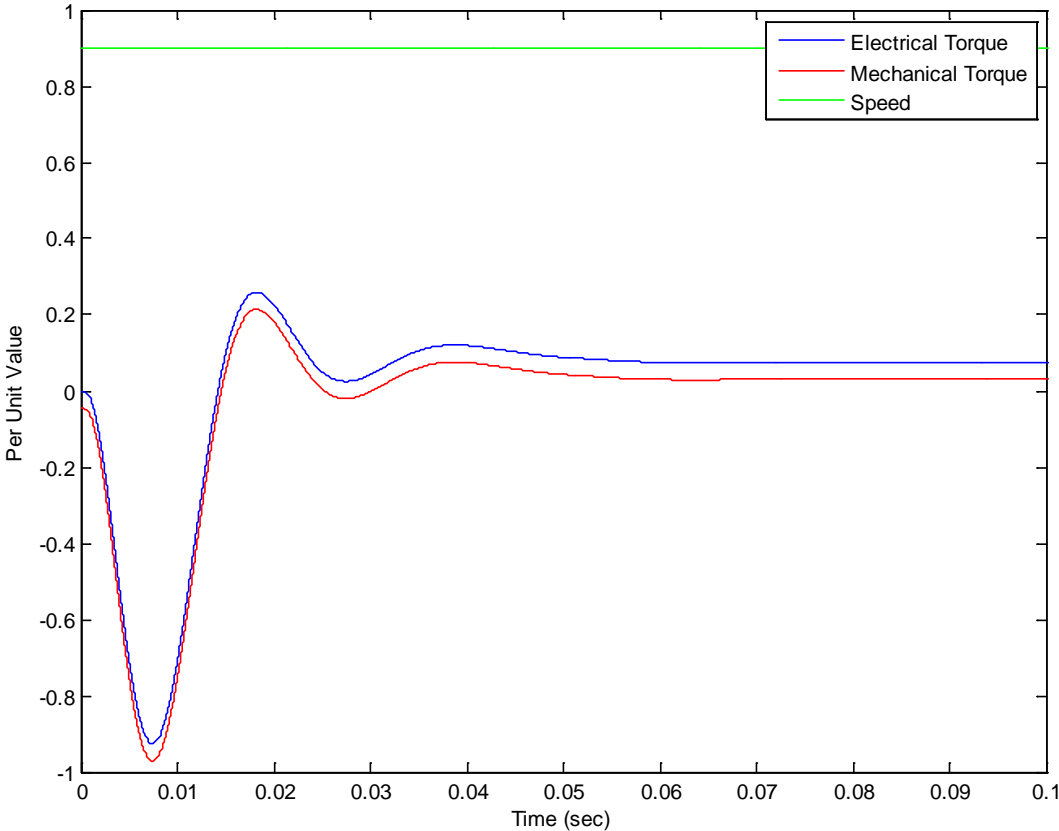


**Figure 4-2.** Speed, Electrical Torque and Mechanical Torque vs. Time During the Transient Period of Simulation

Both the stator current and rotor current was measured as can be seen from Figure 4-1. This is illustrated in Figure 4-3.

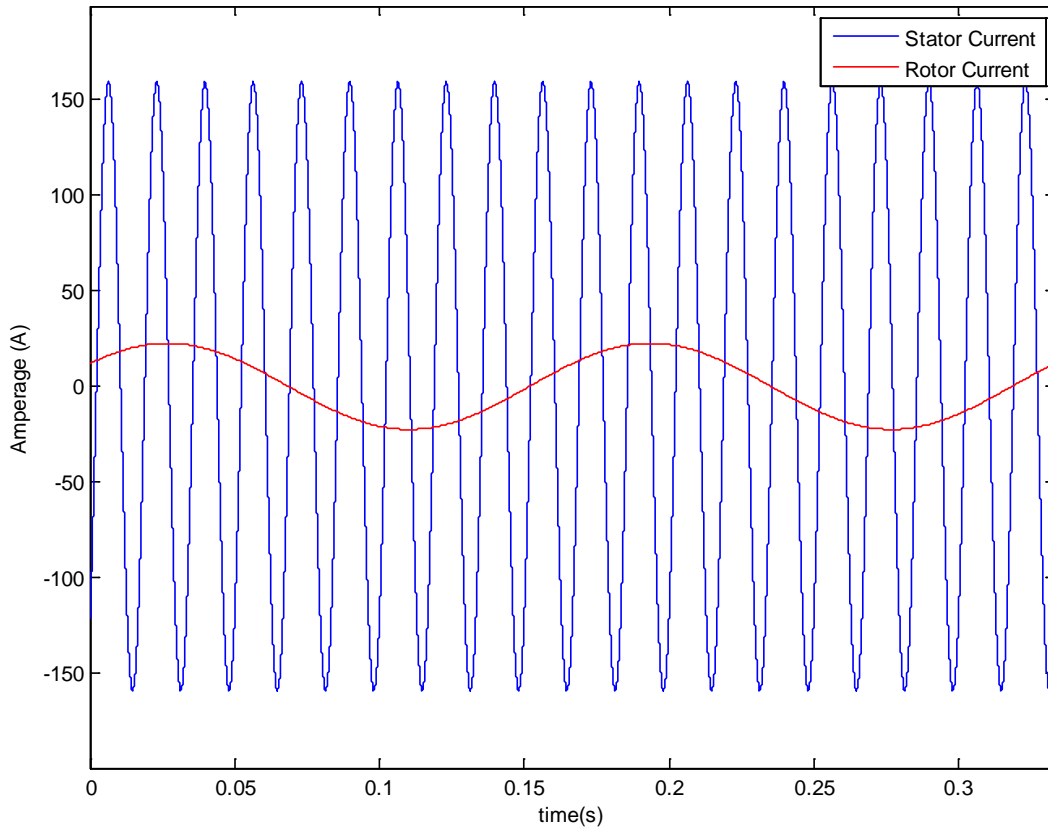


**Figure 4-3.** Stead State Motor Stator and Rotor Currents after Transient Effects have Terminated

It should be noted that in Figure 4-3 that the plot is considering the steady state operation of these currents, therefore the plot considers when the transients die out as time equal to zero seconds.

Finally to confirm that the frequencies of both the stator current and the rotor current were equal to those calculated in equation (4.4) the FFT of the stator current signal and the rotor current were calculated using MATLAB's FFT algorithm. The length of this FFT is 100,000 points. It can be seen from Figure 4-4 that the stator current is equal to the 60 Hz source current as expected and the rotor current is equal to the stator current multiplied by the slip yielding 6 Hz also as expected.

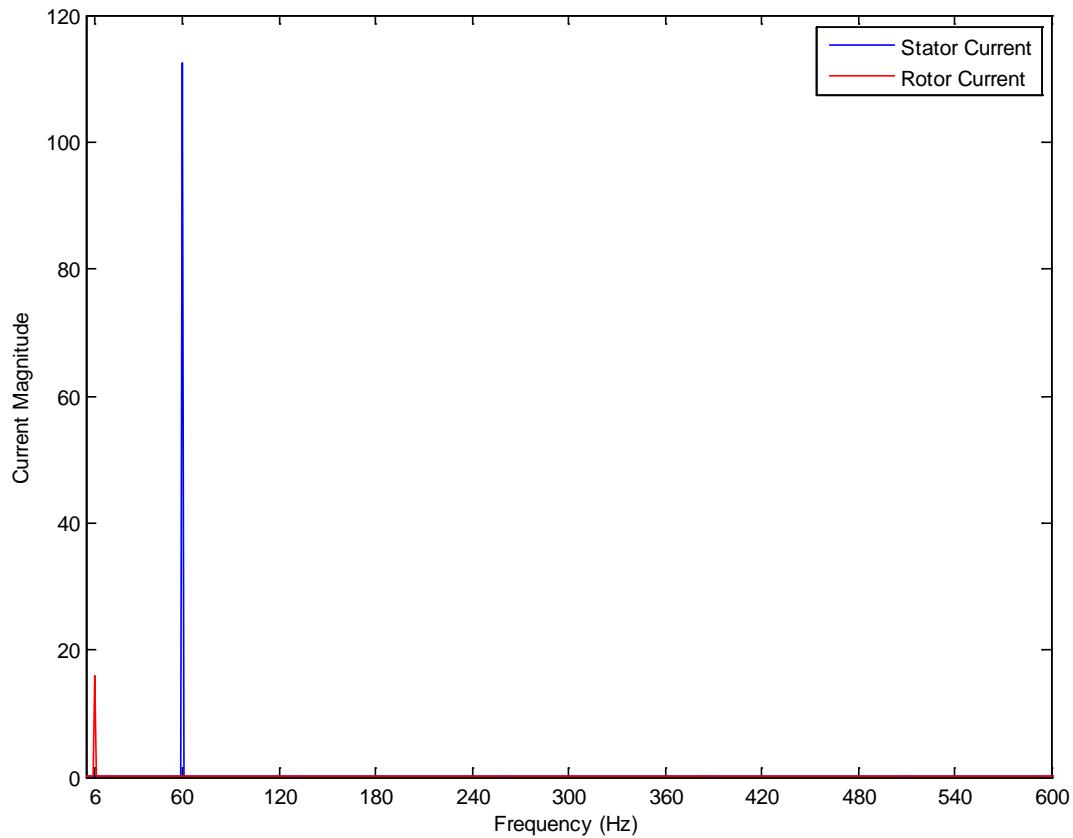


**Figure 4-4.** Single Sided Frequency Spectrum of Stator and Rotor Current

The simulation of the wound-rotor induction motor confirmed the theoretical results that the motors stator current and rotor current would have not only different magnitudes but also frequencies. From this result it can be concluded that rotor frequency which is a fraction of the system's fundamental frequency will be a source sub-harmonics and interharmonics throughout the remainder of the system.

### 4.1.2 Fourier analysis of the Uncontrolled Six-Bridge Rectifier

It can be seen from Figure 3-1 that the rotor windings of the doubly fed induction motor are fed into a three phase rectifier. This section analyzes the behavior of current in a three phase rectifier and how it relates to harmonics. An uncontrolled three-phase rectifier uses six diodes to rectify each phase into a direct current equivalent. This can be seen in Figure 4-5.

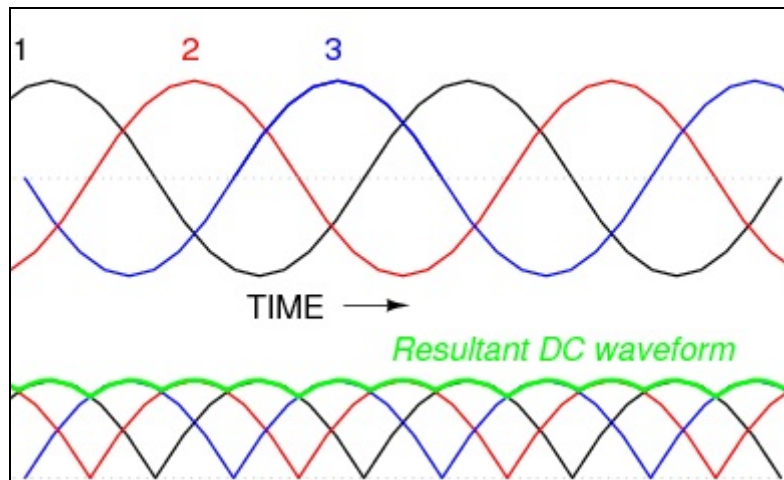


**Figure 4-5.** top: Three-phase Alternating Current Waveform; bottom: Resulting Rectified Direct Current Waveform [40]

By examining the resultant DC waveform in Figure 4-5 one can conclude that the waveform would contain frequencies at six times the fundamental since the rectified waveform has six periods for every fundamental period of the each phase of the AC waveform. Also one could conclude that there will be a large DC harmonic. However, there is a good deal of ripple in a circuit that only uses diodes to rectify the current or voltage. To reduce ripple the resulting waveform can be filtered by the use of an inductor to smooth current waveforms or a capacitor to smooth voltage waveforms. An inductor was chosen because this study is concerned with current

harmonics. It should be noted that this inductor will further distort the DC waveform shown in Figure 4-5.

Figure 4-6 shows the PSCAD circuit that was constructed to simulate a three-phase rectifier. The source is a three-phase, 60 Hz, 460 V<sub>L-L</sub> voltage source. The inductor is a 10 mH inductor that was chosen through trial and error. Increasing the value of this inductor will continue to reduce ripple in the output current waveform; however, a large inductor will slow the response time of the circuit. Therefore, an inductor value must be chosen that both reduces the ripple of the output waveform and has a fast enough response time. For this study 10 mH was adequate.

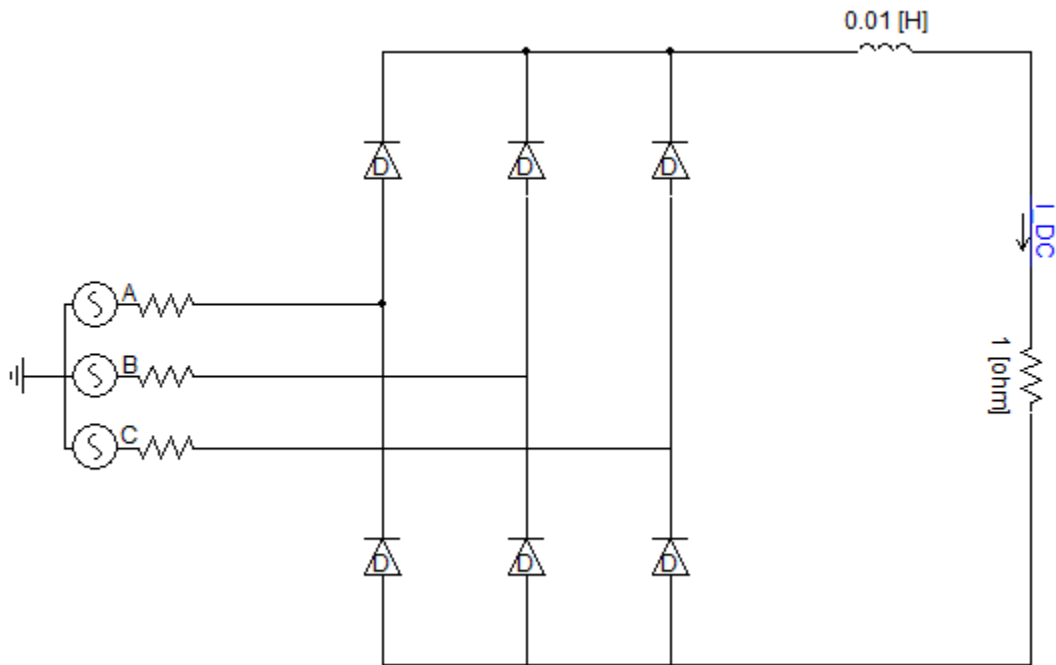


**Figure 4-6.** PSCAD Circuit of a Three-Phase Rectifier

The simulation length was three seconds long to ensure that all transients have died out. This is verified in Figure 4-7. It can be seen that at time equal to zero the inductor begins

charging up because a DC current is applied to it. The inductor then charges to full capacity and acts as a short circuit as expected from DC circuit theory. This transient effect occurs and dies out much earlier than the first tick of 0.05 s. Figure 4-7 illustrates that the three phase current is indeed rectified into a DC current; however, some ripple in the DC waveform can still be observed.

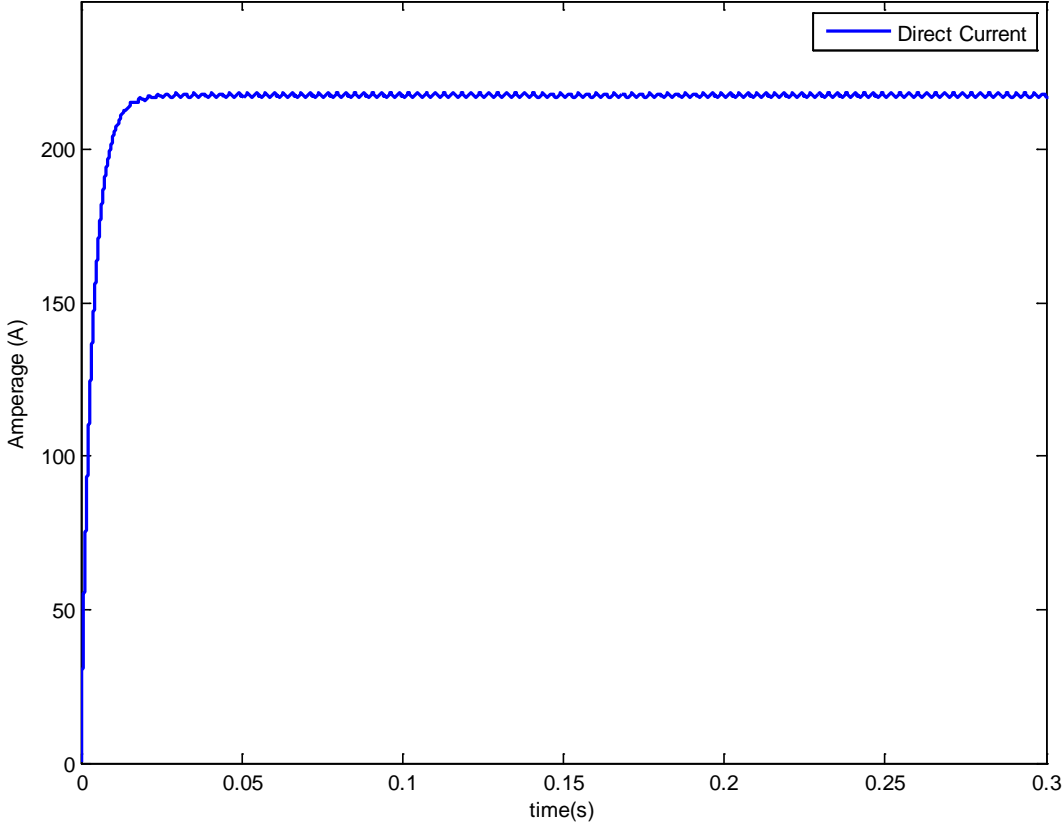


**Figure 4-7.** Illustration of the First 0.3 Seconds of the Three-Phase Rectifier Circuit

The ripple in this circuit can be observed more closely in Figure 4-8. It can be seen from this figure that while the ripple is only a small percentage of the total DC value it still is more

than one amp. It can also be seen from Figure 4-8 that the waveform is distorted from the rectified waveform without the use of a smoothing inductor as was shown in Figure 4-5. This further distortion will add to interharmonic content.

The harmonic spectrum of the three-phase rectifier circuit is illustrated in Figure 4-9. It can be seen from Figure 4-9 that most of the signal's energy is concentrated at its DC value as would be expected for a DC circuit. The majority of the remaining energy for the signal is concentrated in the frequencies which are an integer multiple of 360 Hz which is the fundamental frequency for a rectified three-phase waveform. The fundamental frequency of the rectified waveform is six times that of the 60 Hz input to the system as was expected.

These integer multiples of 360 Hz are also integer multiples of the 60 Hz system so they fall into the class of classical harmonics which are integer multiples of the fundamental frequency. However to see if there are energy in frequencies that are not an integer multiple of the 60 Hz system frequency the y-axis of Figure 4-9 was reduced.

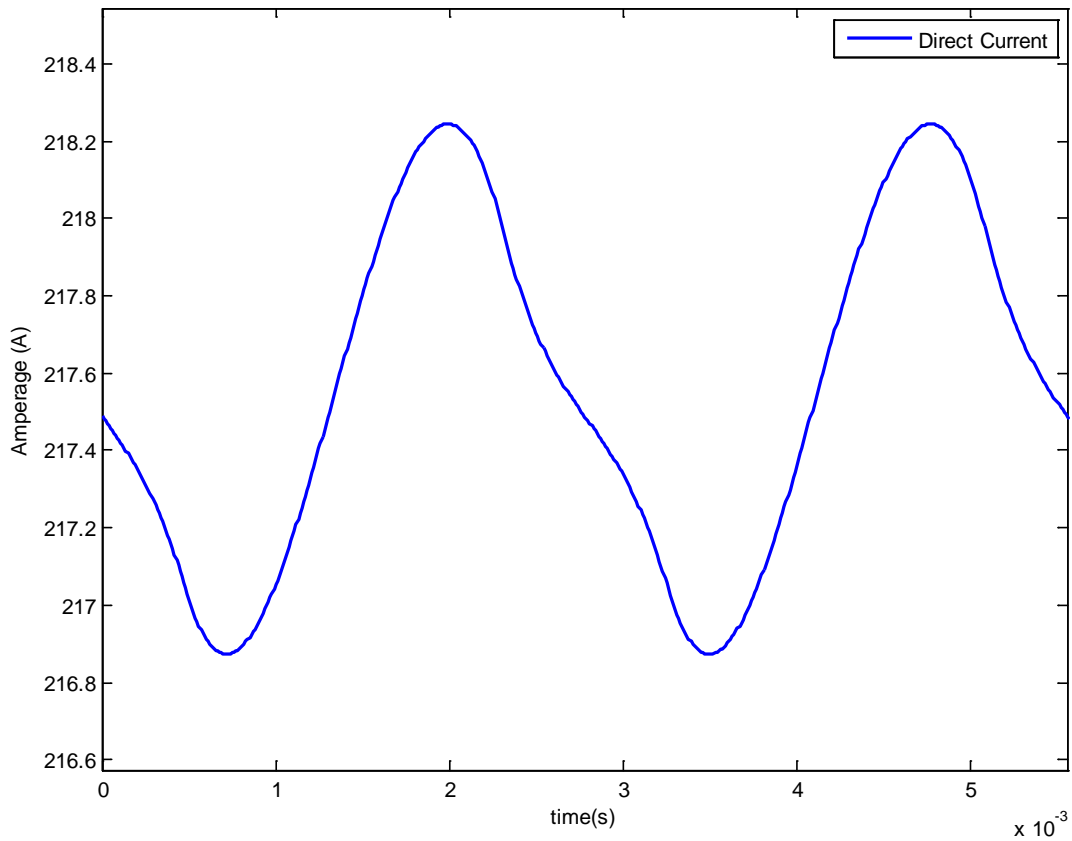


**Figure 4-8.** DC Current Ripple in Three-Phase Rectifier Circuit

Figure 4-10 illustrates the frequency spectrum of the three-phase rectifier circuit with the y-axis reduced. The maximum value of the y-axis for this plot is 100  $\mu$ A. It can be seen from Figure 4-10 that there is energy at sub-harmonic and interharmonic frequencies. Besides the DC component and the integer multiples of 360 Hz the two frequencies that contain the most energy are slightly greater than and slightly less than 60 Hz respectively.

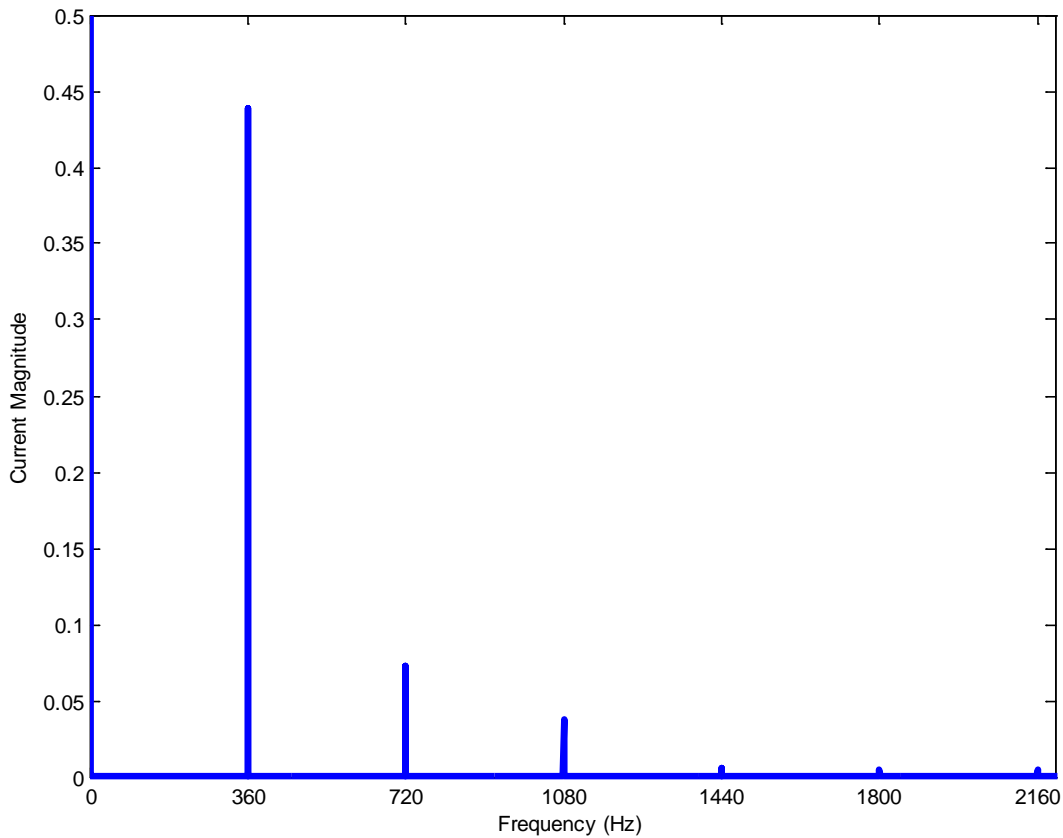


**Figure 4-9.** Single Sided Frequency Spectrum of the Three-Phase Rectifier Circuit

While these sub-harmonics and interharmonics range in between  $10 \mu\text{A}$  and  $50 \mu\text{A}$  and most likely will not be harmful to power systems components with large power ratings. These components cause erroneous readings in measurement equipment or other communications circuits.

The three-phase rectifier circuit rectifies each phase of an alternating current signal and yields a DC current with ripple. The ripple DC resultant waveform is then reduced by an inductor which in turn slightly distorts the waveform but does reduce the ripple. The harmonics spectrum of resultant DC waveform contains sub-harmonics, interharmonics and harmonics of integer multiples of the fundamental AC source.

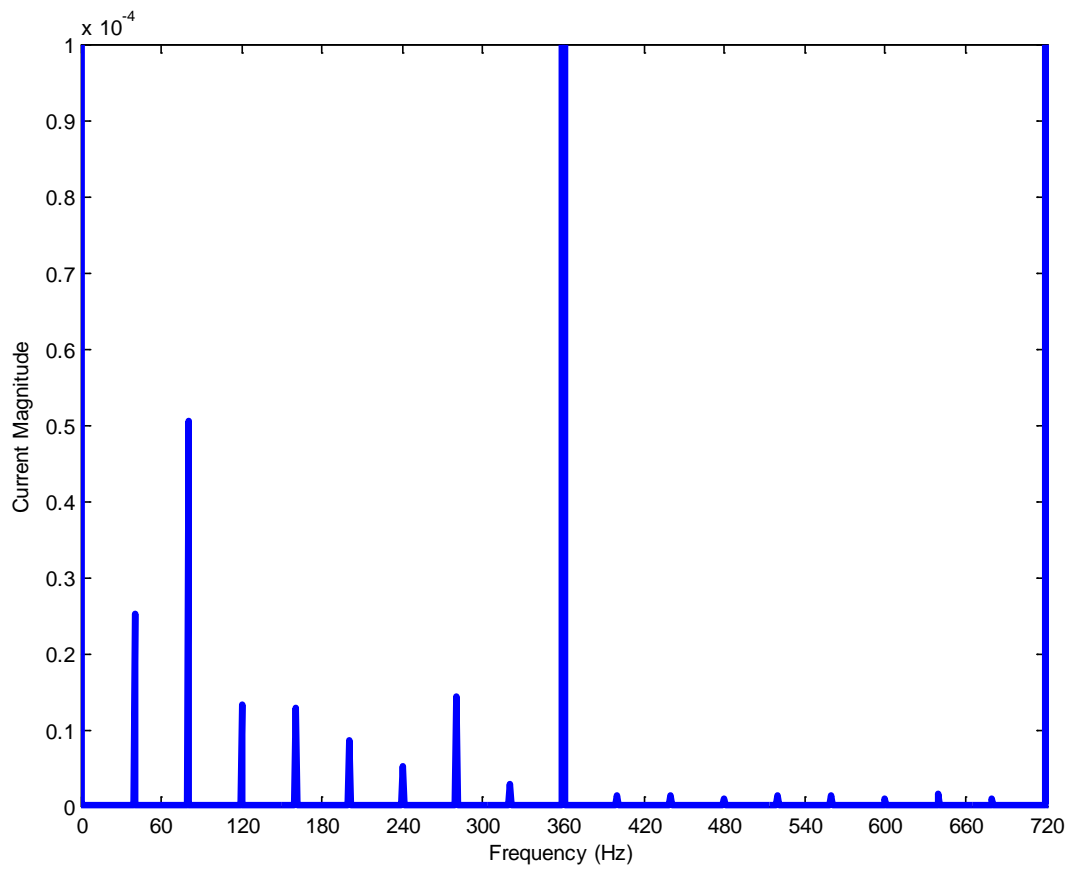


**Figure 4-10.** Illustration of Sub-Harmonics and Interharmonics for the Three-Phase Rectifier Circuit

While the majority of the energy is focused in the DC component of the resulting DC waveform as desired, it was shown in this simulation that there is a significant harmonic component of the waveform and a small contribution from the sub-harmonic and interharmonic components.

### 4.1.3 Fourier analysis of the Three-Phase Inverter

Figure 3-1 shows that the three-phase rectifier that feeds the three-phase inverter with its rectified DC current. This section describes the behavior of the three-phase inverter used in the static Kramer drive system and analyzes the inverter's frequency spectrum.

The schematic diagram of the three-phase inverter can be seen from the PSCAD circuit given in Figure 4-11.

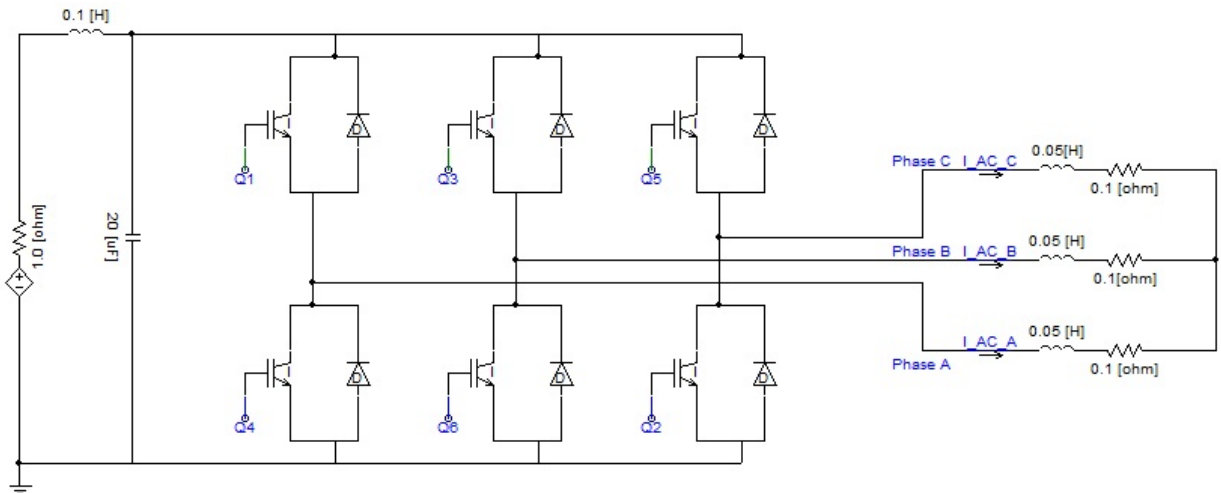


**Figure 4-11.** Three-phase Inverter PSCAD Schematic

The circuit contains a 460 V direct current source, six IGBTs labeled as  $Q_1$  through  $Q_6$ , and a smoothing inductive filter for each of the phase. Figure 4-12 illustrates the firing sequence for each of the transistors and the voltage waveform that results. The square wave current that is produced in turn yields a three phase 60 Hz sinusoidal current. The current is of course not a perfect sinusoid and contains harmonic distortion. The resulting three phase current waveform can be seen in Figure 4-13.

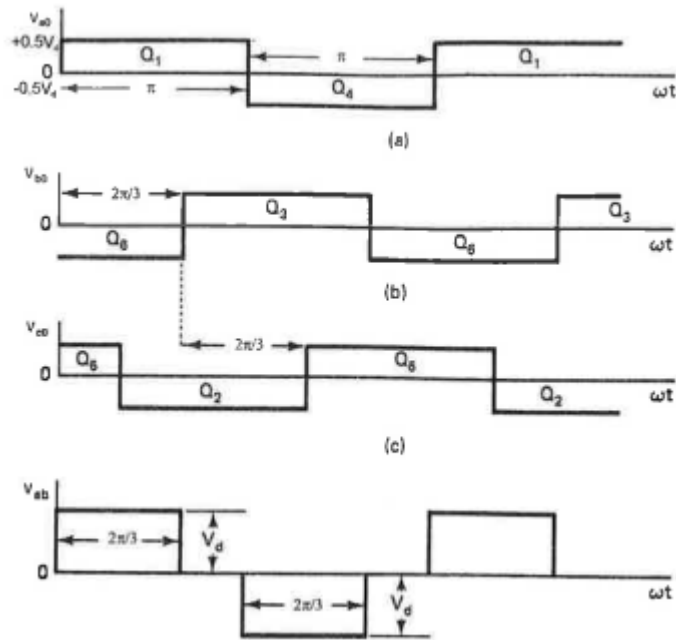


**Figure 4-12.** Transistor Firing Sequence and Resultant Line to Line Voltage Waveform

The simulation was run for 3 seconds. Figure 4-13 captures the last two cycles of the simulation. It is shown in this simulation that there are three phases of current which appear to be displaced by  $120^\circ$  from each other. These waveforms appear to have some harmonic distortion in them. To more clearly see the effect of harmonic distortion, only one phase the inverter is plotted. This can be seen from Figure 4-14.

The phase A current that is plotted in Figure 4-14, was analyzed for its frequency components. The FFT of the signal was taken using MATLAB and its single sided frequency spectrum is plotted in Figure 4-16. It can be seen from this figure that the majority of the energy in the signal has a frequency of 60 Hz as expected. However, there is a significant amount of energy that lies in the fifth harmonic at 300 Hz.

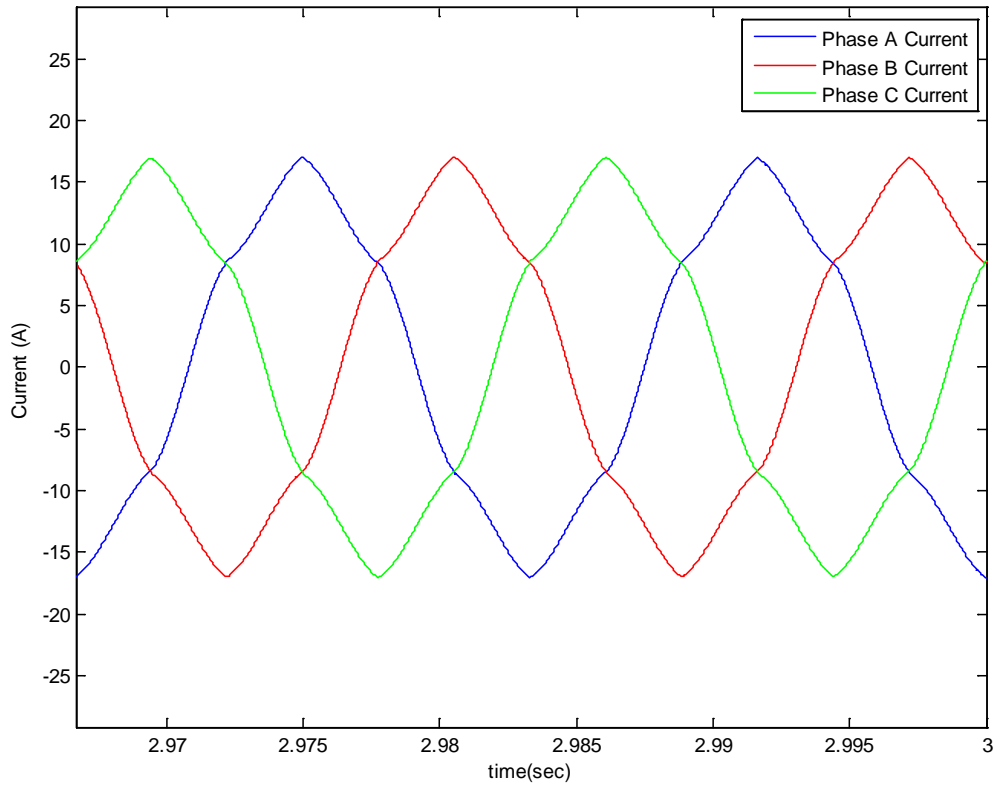


**Figure 4-13.** Inverted Three-Phase Current

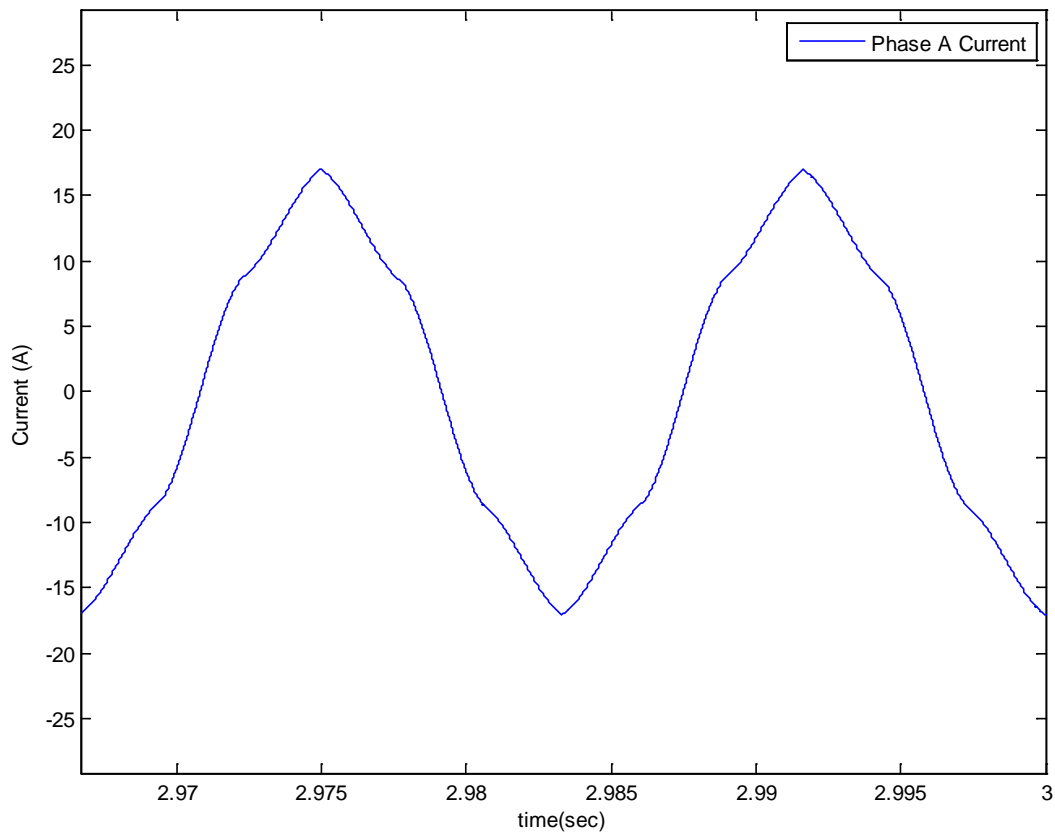


**Figure 4-14.** Inverted Phase A Current

Figure 4-15 has a scale in which the only harmonics that can be seen are the fundamental component at 60 Hz and the fifth harmonic at 300 Hz. To examine any sub-harmonic and interharmonic components the scale of the figure must be changed. Figure 4-16 reduces the scale enough so that these interharmonic components can be observed. It can be seen from this figure that there are interharmonic components in between each of the first five harmonics which have a significant contribution to the total harmonic distortion. It can also be seen from this figure that there is a seventh harmonic contribution to the total harmonic distribution.

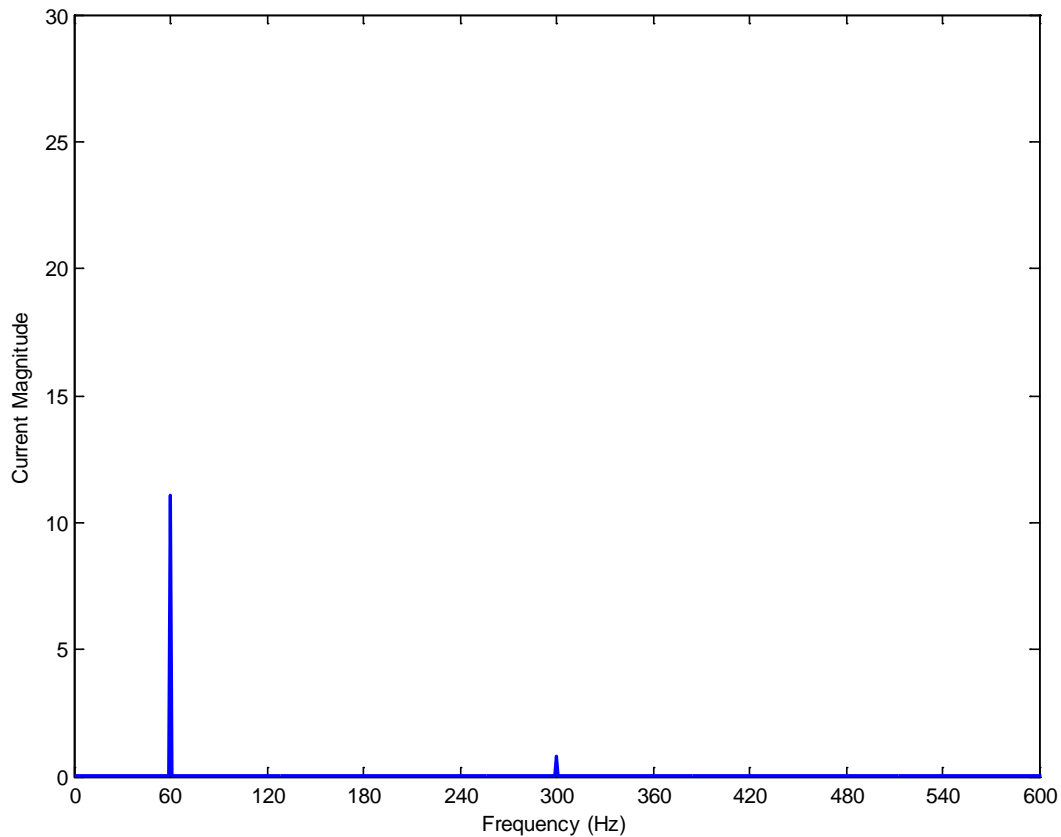


**Figure 4-15.** Single Sided Frequency Spectrum of Three Phase Inverter

The three phase inverter takes a direct current source and converts that source to a three phase alternating current signal. It would be ideal for the three-phase output signal to be a sinusoid only composed of a fundamental frequency. However, as with all power electronic non-linear systems there are harmonics generated. As was shown in this simulation the vast majority of the energy in the three-phase inverter is concentrated in the fundamental with a smaller but still significant contribution of energy lying in the fifth harmonic. On a much smaller level there is the existence of sub-harmonic and interharmonic components. While the magnitude of these sub-harmonic and interharmonic components most likely not large enough to damage large

power system equipment they are significant enough to effect communications equipment such as transmitters.

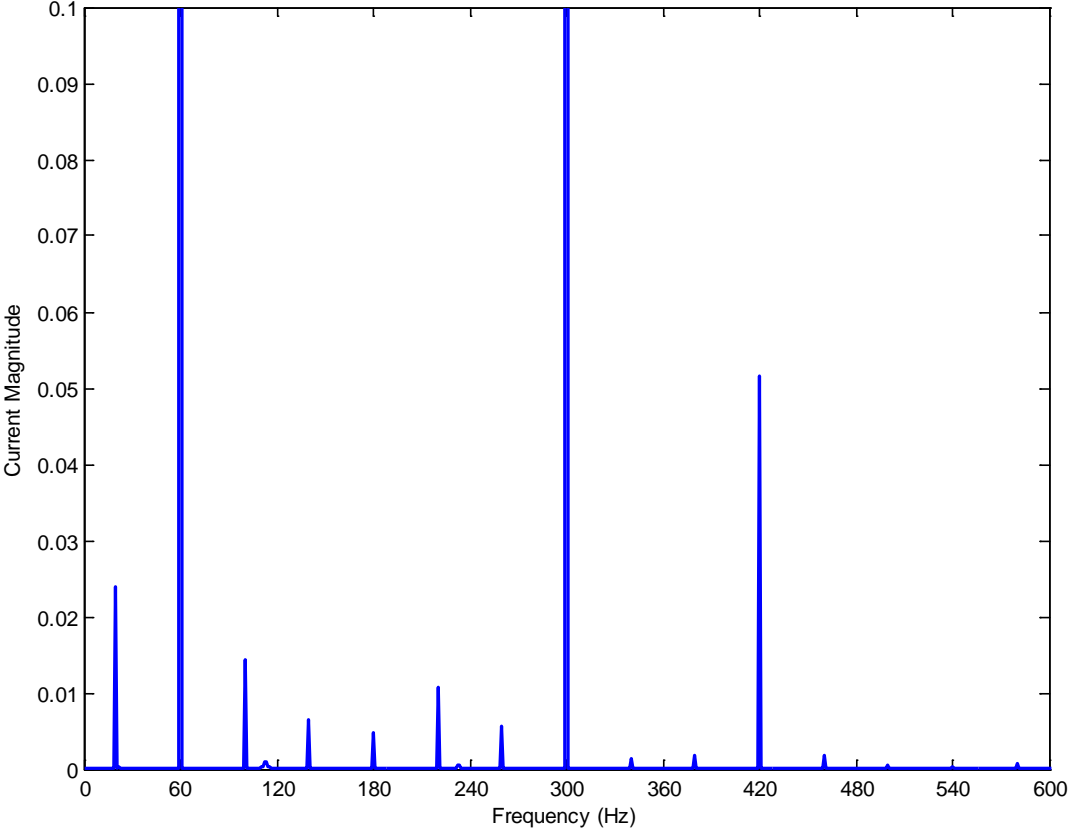


**Figure 4-16.** Single Sided Frequency Spectrum of Three-Phase Inverter with Interharmonic Components

These harmonic, sub-harmonic and interharmonic components can cause significant problems in the static Kramer drive system especially after they are fed through a transformer and amplified by some degree. The results found in this section will aid in further analysis and estimation.

#### 4.1.4 Fourier analysis of a Three-phase Transformer System

The final component of the static Kramer drive system is a three-phase transformer. The three-phase transformer operates under the same principle as the single-phase transformer however there is some phase shift associated with the delta-wye or wye-delta connections. For this simulation a wye-delta grounded transformer was chosen. The wiring diagram for a wye-delta grounded transformer can be seen in Figure 4-17.

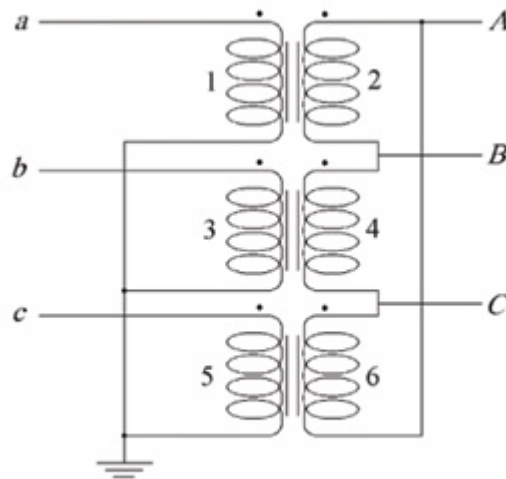


**Figure 4-17.** Wiring Diagram for a Wye-Delta Grounded Transformer

The PSCAD schematic diagram is shown in Figure 4-18. The transformer is rated at 34.5 KVA and has a voltage turns ratio of 115/460 V<sub>L-L</sub>. The circuit was simulated using PSCAD and

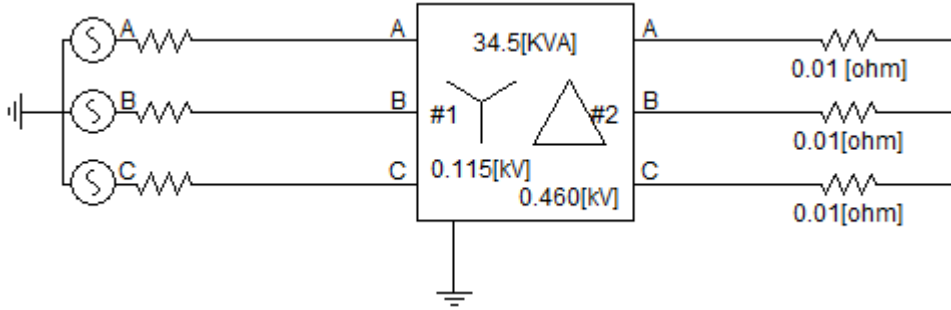


**Figure 4-18.** PSCAD Schematic Diagram for Three Phase Transformer

the data was plotted using MATLAB. Both the line current for the primary and secondary circuits was simulated. These signals can be seen plotted in Figure 4-19.

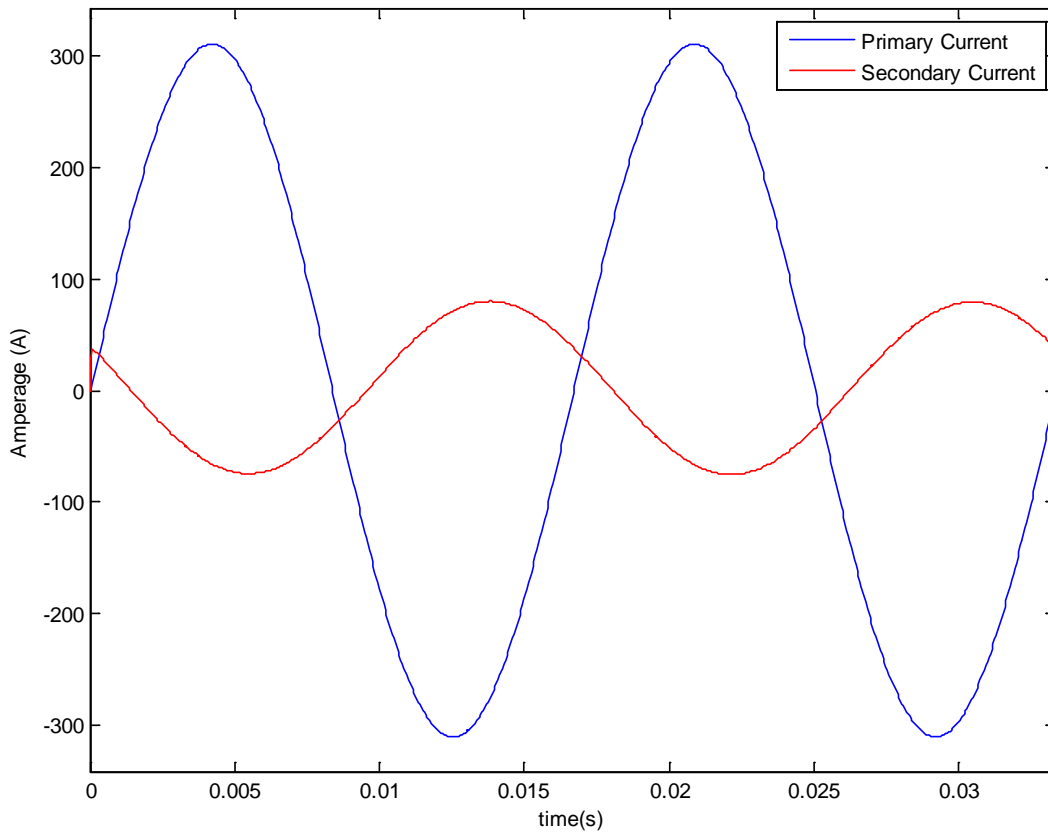


**Figure 4-19.** Primary and Secondary Current for the Wye-Delta Transformer

It can be seen from the plot that the secondary current is simply a fraction of the primary current with a  $30^\circ$  phase shift. It should be noted that this is only one phase of the primary and one phase of the secondary currents. Since the voltage ratio is 1:4 in a step up fashion, the current ratio is therefore 4:1 in a step down fashion. This can also be verified through Figure 4-19. Lastly the frequency spectrum for the three phase transformer was plotted and can be seen in Figure 4-20. It should be noted from this figure that there is not a significant contribution to these signals in any frequency other than the fundamental.

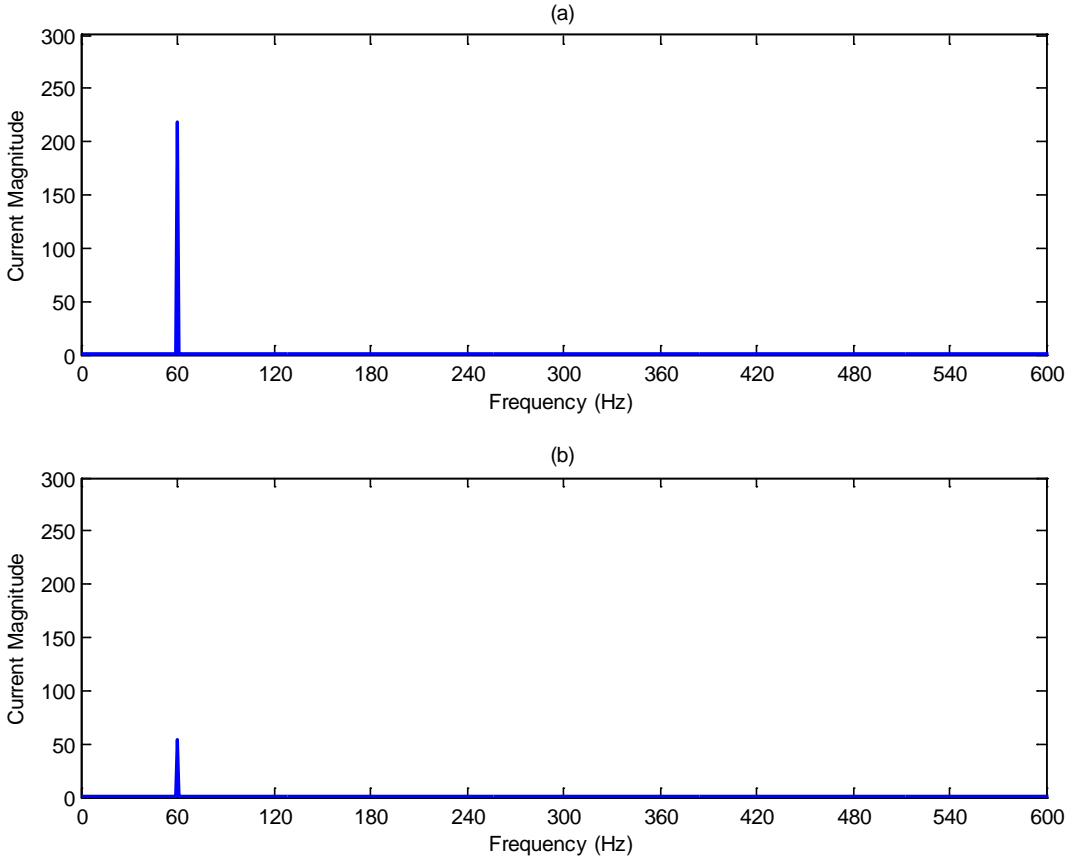


**Figure 4-20.** Single Sided Frequency Spectrum for Primary Current (a); Single Sided Frequency Spectrum for Secondary Current (b)

The three-phase transformer is the last element in the static Kramer drive system. It steps voltage up and in turn steps current down. There are mainly only contributions from the fundamental frequency as was shown in these simulation results. However it should be noted that any harmonic or interharmonic components that are fed into the transformer will end up on the secondary side of the transformer and back into the system.

## **5.0 SYSTEM SIMULATION**

This section describes the results of the static Kramer drive system once the system was completed and put all together. Due to the fact that there were some limitations in PSCAD both in number of busses aloud in the student version and its limitations regarding its Fourier analysis tools the total system was built and simulated using MATLAB. The MATLAB tool that was used for this simulation was SimPowerSystems. SimPowerSystems is a sub-package of Simscape which is a sub-package of Simulink.

### **5.1 CONSTRUCTION OF THE STATIC KRAMER DRIVE SYSTEM IN SIMPOWERSYSTEMS**

The static Kramer drive system that is illustrated in Figure 3-1 was constructed in SimPowerSystems as was previously mention. The overall system that was constructed can be seen in Figure 5-1.

It can be seen from this figure that the model is constructed of several components. From left to right the first component of the system is a three-phase 460 V<sub>LL</sub>, 60 Hz, 184 KVA source, which had an X/R ratio of 5.

The next component in the system was a simple measurement device. The device used is a three-phase measurement device which is set to measure the three-phase voltage as a phase to ground measurement and the three-phase current flowing through the device.

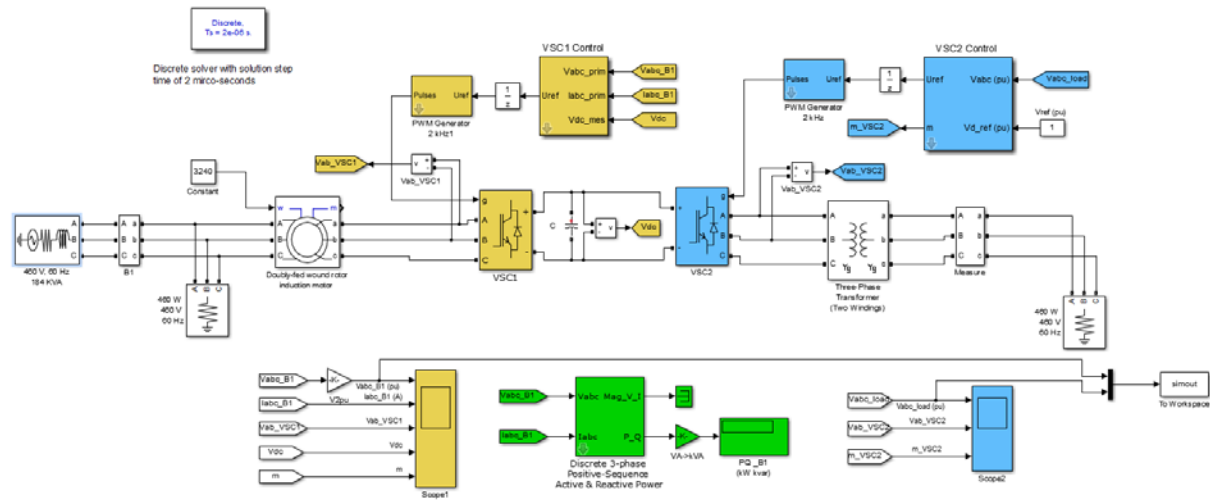


**Figure 5-1.** SimPowerSystems Model of Static Kramer Drive System

The next component of the model is a three-phase parallel RLC load. It can be seen from Figure 5-1 that this load is simply resistive. The reason that this load is used in the SimPowerSystems model but is not seen in the traditional static Kramer drive schematic is because it is needed to keep the model stable. SimPowerSystems will not permit a voltage source to be connected to a wound rotor induction machine because the voltage source is obviously treated as a voltage source but the induction machine is treated as a current source. This causes a problem with the way that the simulation is solved and would not permit the system to be solved. Hence, the solution to this problem was to put large resistance which would draw virtually no current, keeping the system virtually the same in parallel with either the motor or the source. The

current that is being drawn by this parallel load can be seen in Figure 5-2. It should be noted that this current is less than one amp which can effectively be considered zero for this study.

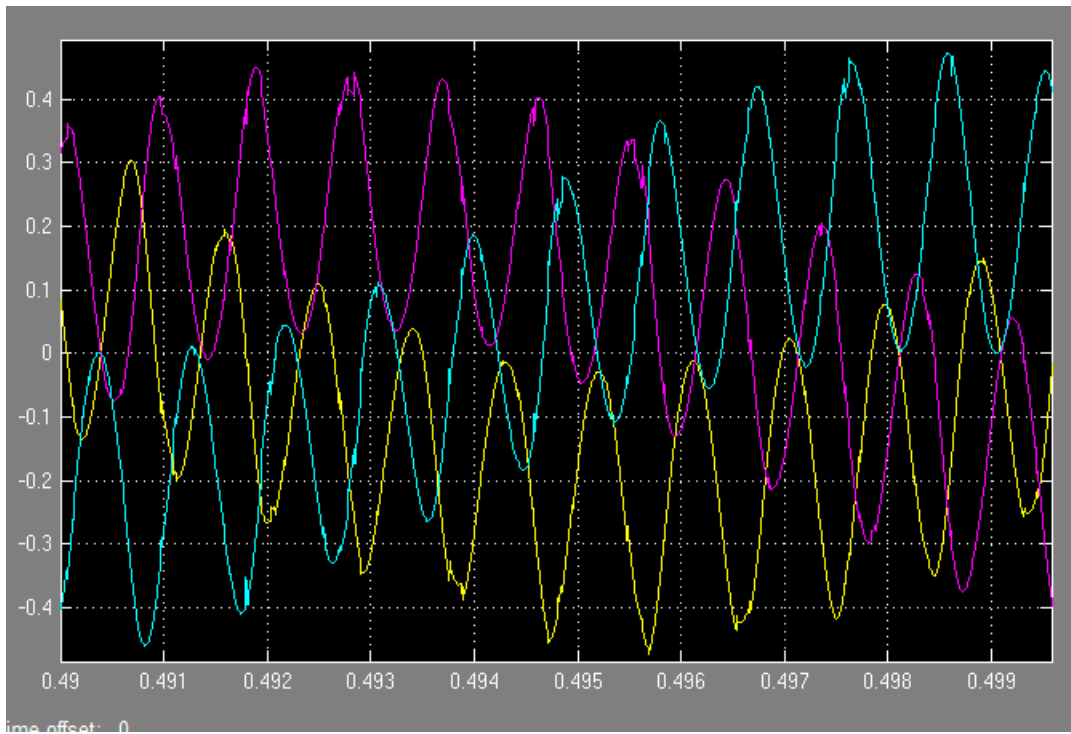


**Figure 5-2.** Current Drawn by the Stabilizing Resistive Load

The next component in this system is the wound rotor induction motor. The motor in this system is a 2-pole, 460 V<sub>LL</sub>, 150 Hp motor. The stator resistance and inductance of the motor were 0.029  $\Omega$  and 60 mH respectively. The rotor resistance and inductance of the motor were 0.022  $\Omega$  and 60 mH respectively. The mutual inductance of the machine was 34.5 mH. The motor was run in speed control mode with the speed set at 3240 rpm which is equivalent to 90% of the synchronous speed of a two-pole machine. This is the same speed that the motor was run in the PSCAD simulation done in 4.1.1. The motor being run at this speed resulted in a 6 Hz output voltage on the rotor windings.

The next component of the model was a three-phase rectifier which converted the output voltage signal from the induction motor into a direct current voltage signal. The converter that was used a three-bridge universal bridge IGBT. The control strategy that was used for this converter was the same control strategy that was used in [41]. This strategy used was pulse width modulation with pulses being sent the device at 2 KHz.

The direct current output of the converter had a capacitor connected to the positive and negative terminals of the device which was used to smooth out the direct current waveform. The size of the capacitor used was 1800  $\mu\text{F}$ .

The direct current output of the rectifier was smoothed out by the aforementioned capacitor and then fed into another power converter. This time the converter was an inverter which was composed of the same three-bridge universal bridge IGBT as the rectifier. Also this inverter used the control strategy derived in [41].

After the three phase inverter the voltage is stepped back up to the original 460  $V_{LL}$  level that the original system was operating at. The voltage was stepped up via a three-phase Y-Y grounded transformer.

The last component in the static Kramer drive system was a simple load which is connected to ground, thus completing the static Kramer drive system's loop that was illustrated in Figure 3-1. The load is a simple real power resistive load which draws 460 W at 460  $V_{LL}$  and is placed in parallel with the static Kramer drive circuit.

## 5.2 PERFORMANCE OF THE STATIC KRAMER DRIVE CIRCUIT

The section analyzes the performance of the static Kramer drive circuit showing the significant problems of harmonics and interharmonics that were expected from the component by component analysis that was performed on each component of the system. The voltage and current waveforms of the source can be seen in Figure 5-3. The top waveform is the per-unit phase-to-ground measurements for source voltage. The middle waveform is the per-unit current flowing through the measurement device and through measurement device. The bottom waveform is the line-to-line voltage that is read from the phase A to phase B.

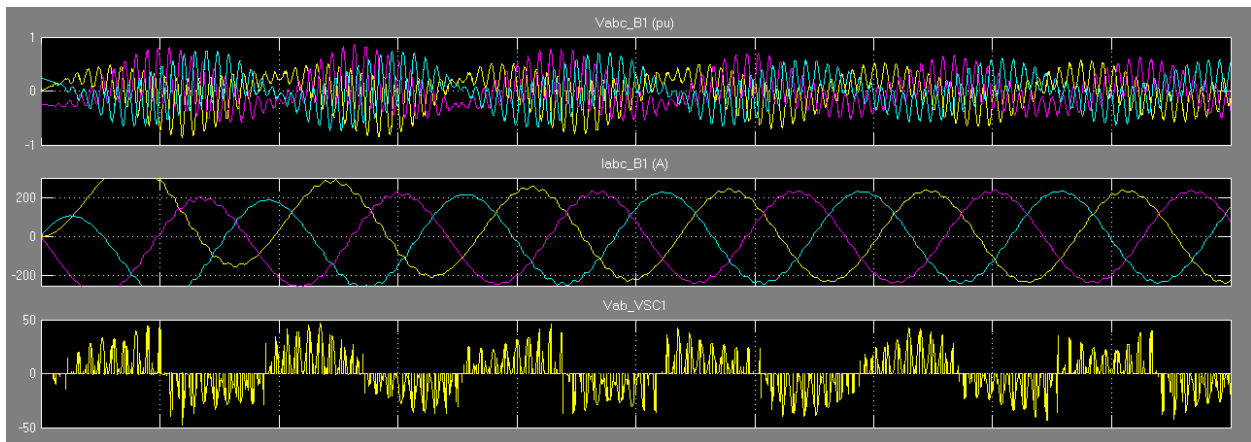


**Figure 5-3.** Voltage and Current Waveforms Measured from the Source

It can be seen in all of these waveforms that there is some distortion caused by the system that the source is feeding. This can be seen in the most detail in the voltage waveforms. In fact, it appears that the 60 Hz voltage wave is enveloping a much higher frequency waveform. This follows the expected prediction from the component-by-component analysis that was performed in the previous chapter.

The next waveform that was analyzed was the direct-current voltage waveform that was flowing in-between the power converters. This waveform can be seen in Figure 5-4. It should be noted that there is a large total harmonic distortion.

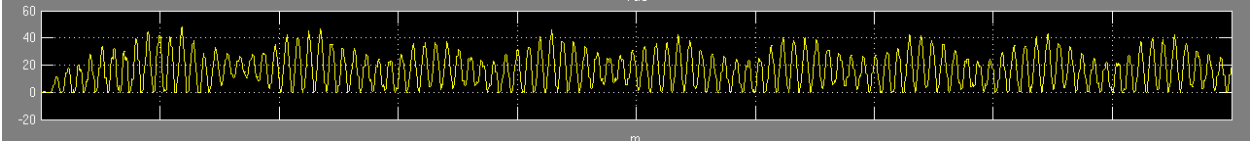


**Figure 5-4.** Rectified Direct Current Waveform with Strong Harmonics Present

The next waveform that was measured in the system was the three-phase voltage output of the inverter. This waveform can be seen in Figure 5-5.

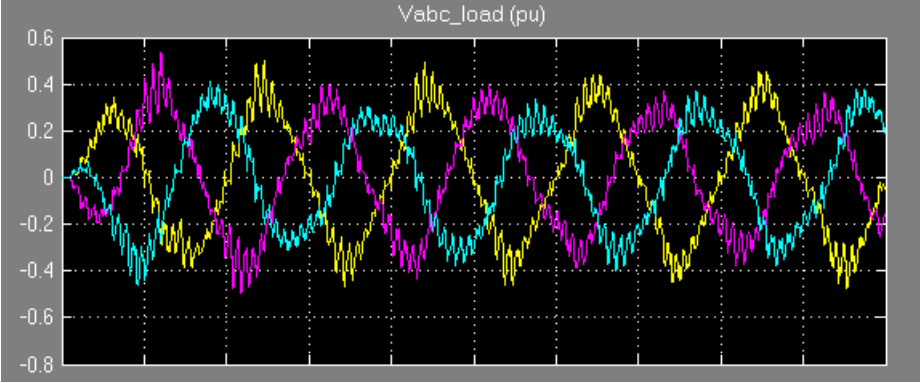


**Figure 5-5.** Output Waveform Sent Back to the System Load

It should be noted that in this output waveform has a great deal of total harmonic distortion. It is clear that for this voltage wave there are at least two very distinct frequencies.

The last and final waveform that was analyzed is the phase-to-phase voltage between phase A and phase B. This waveform also contains a very noticeable amount of total harmonic distortion. This waveform can be seen in Figure 5-6.

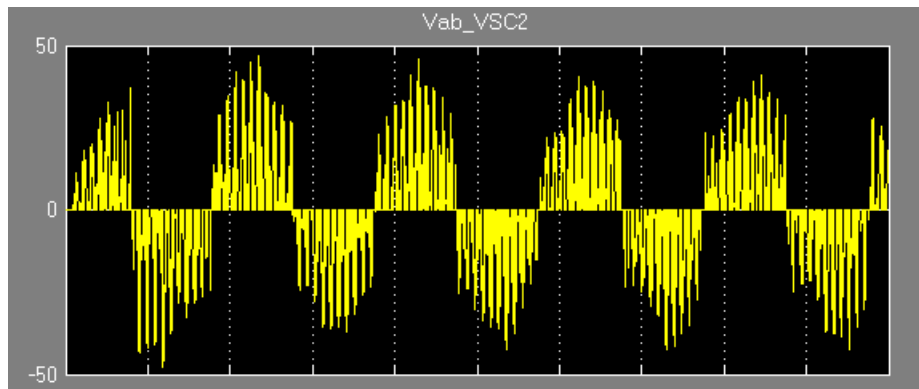


**Figure 5-6.** Phase-to-Phase Voltage of the System Output

### 5.3 EXPORTING SIGNALS INTO MATLAB

The three phase voltage signals for the input and output of the static Kramer drive system were exported from SimPowerSystems back into MATLAB so they could be captured and analyzed via an .m file. These signals were captured using the simout block from Simulink. This can be seen in Figure 5-7.

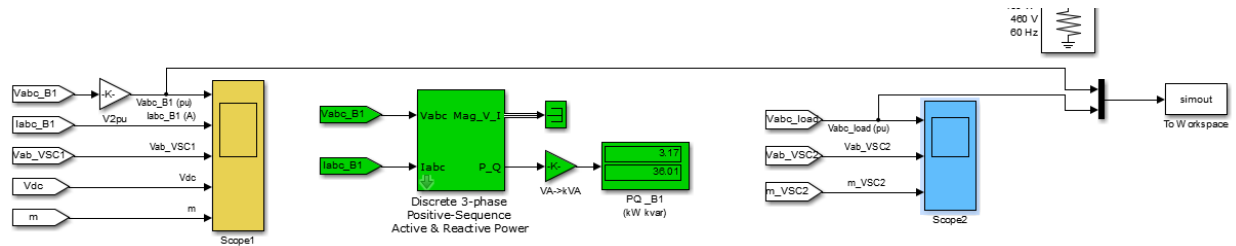


**Figure 5-7.** Capturing Voltage Signals Using the Simout Simulink Block

The signals that were captured were captured in the form of an array with an associated time. The time that was associated with this array was the 2  $\mu$ s. These signals were captured using the simout block and then copied and imported back into a text file. The exported signal can be seen in a text file in Figure 5-8. In the leftmost column the time is contained. This time is incremented in steps of 2  $\mu$ s.

The text file was then used as a file import to MATLAB so that the overall input and output voltage signals could be analyzed. The method of analysis that was performed on the system was the same Fourier analysis that was performed on each component of the system in the previous chapter. Both the input and output voltage signal were plotted in MATLAB and compared against the SimPowerSystems simulation to make sure that everything was converted to text correctly. It can be seen Figure 5-9 where the voltage from the systems source is the top voltage plot and the voltage from the systems output is the bottom voltage plot. These plots agree with the previously simulated results from SimPowerSystems. Once the voltage plots were capture and verified for correctness versus their SimPowerSystems counterparts they could be analyzed for their frequencies.

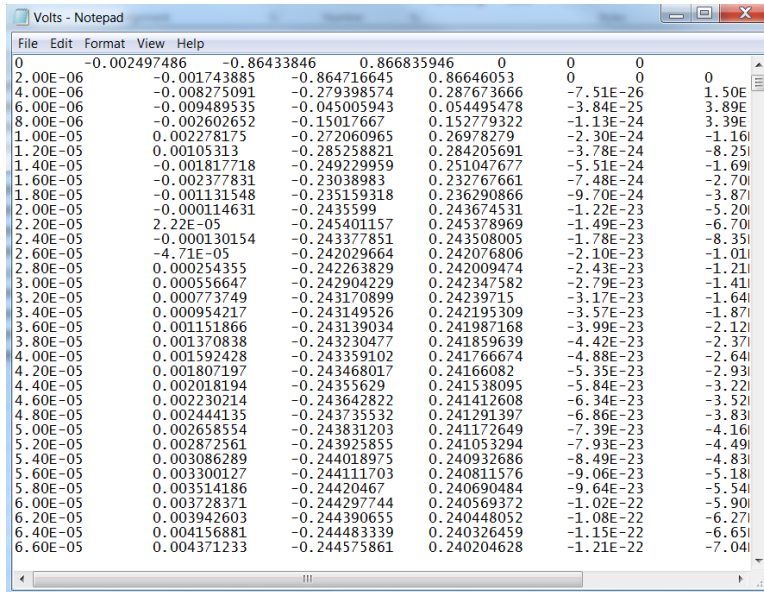


**Figure 5-8.** Text File Containing Input and Output Voltage Readings

The signals that were taken from the text file that is illustrated in Figure 5-8 were then analyzed for their harmonic components.

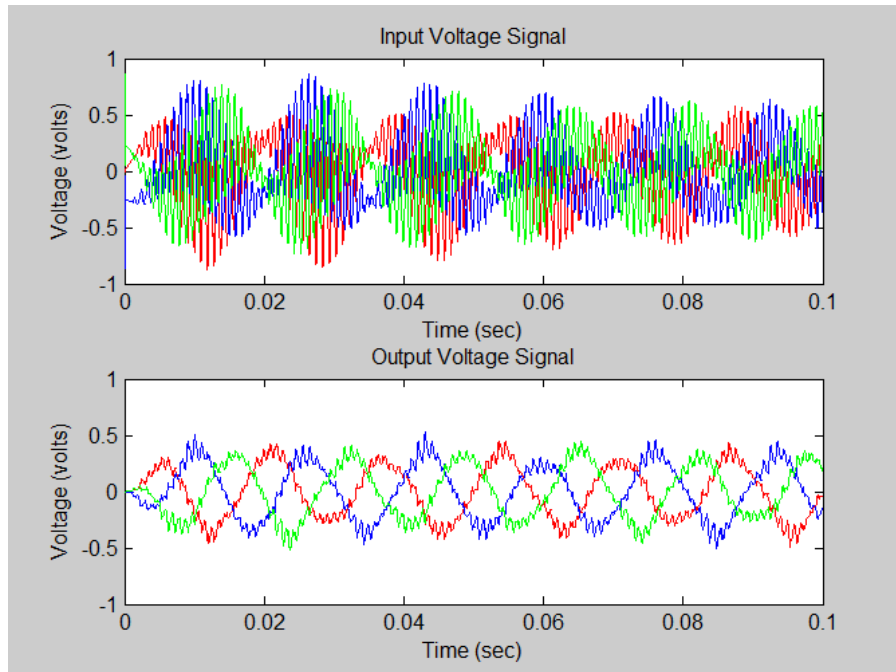


**Figure 5-9.** Voltage from the System's Source (top); Voltage from the System's Output (bottom)

The MATLAB script that was used to analyze these signals for their harmonic components is illustrated below:

```
L = length(time);
Ts = abs(time(2)-time(1));
Fs = 1/Ts;

VOLTAGE_IN = fft(Va_in,L)/L;
VOLTAGE_OUT = fft(Va_out,L)/L;
freq = Fs/2*linspace(0,1,(L/2)+1);

figure(2)
stem(freq,sqrt(2)*abs(VOLTAGE_IN(1:L/2+1)))
axis([0 200 0 25*sqrt(2)*max(VOLTAGE_IN)])
title('Single-Sided Amplitude Spectrum of Input Voltage Signal')
xlabel('Frequency (Hz)')
ylabel('Voltage Magnitude')
```

This script takes the signal and performs the fast Fourier transform of the signal so that it can be analyzed for its harmonic components. The output results for this script can be seen in

Figure 5-10. We can see that the input signal has very little harmonic distortion in the frequencies that surround the fundamental 60 Hz frequency however the output signal has a great deal of sub-harmonic and interharmonic distortion. We can see that when changing the x axis of the plots in Figure 5-10 that there is some significant harmonic distortion in the input signal at very high frequencies that are much larger than the fundamental 60 Hz signal.

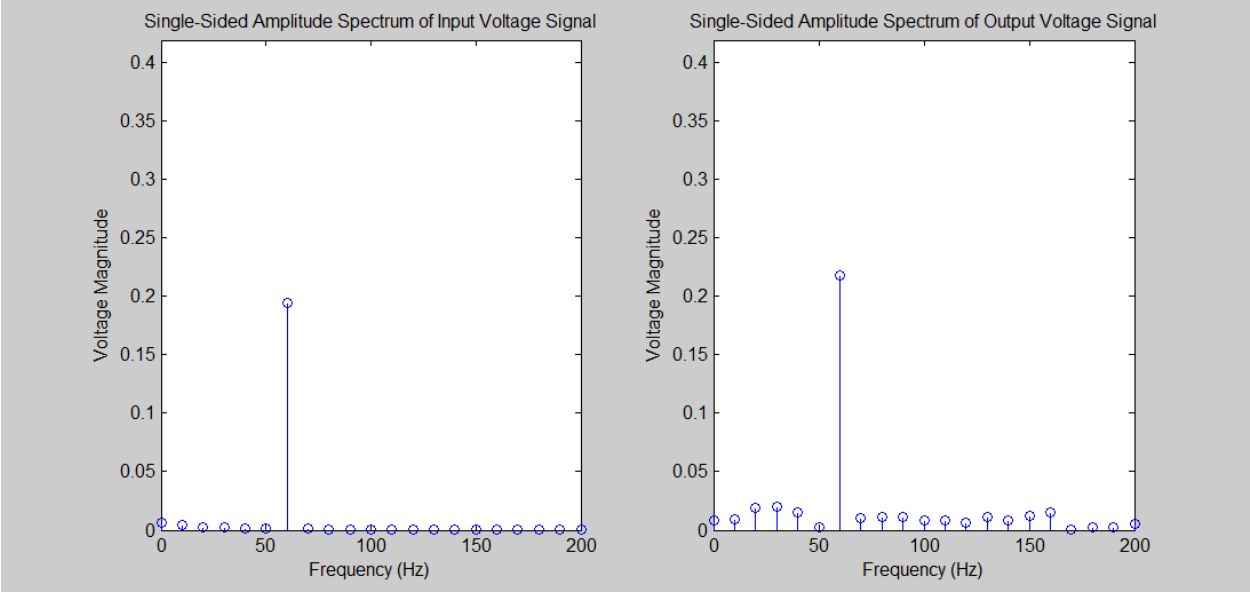


**Figure 5-10.** Fast Fourier Transform of the Input and Output Signal for the System

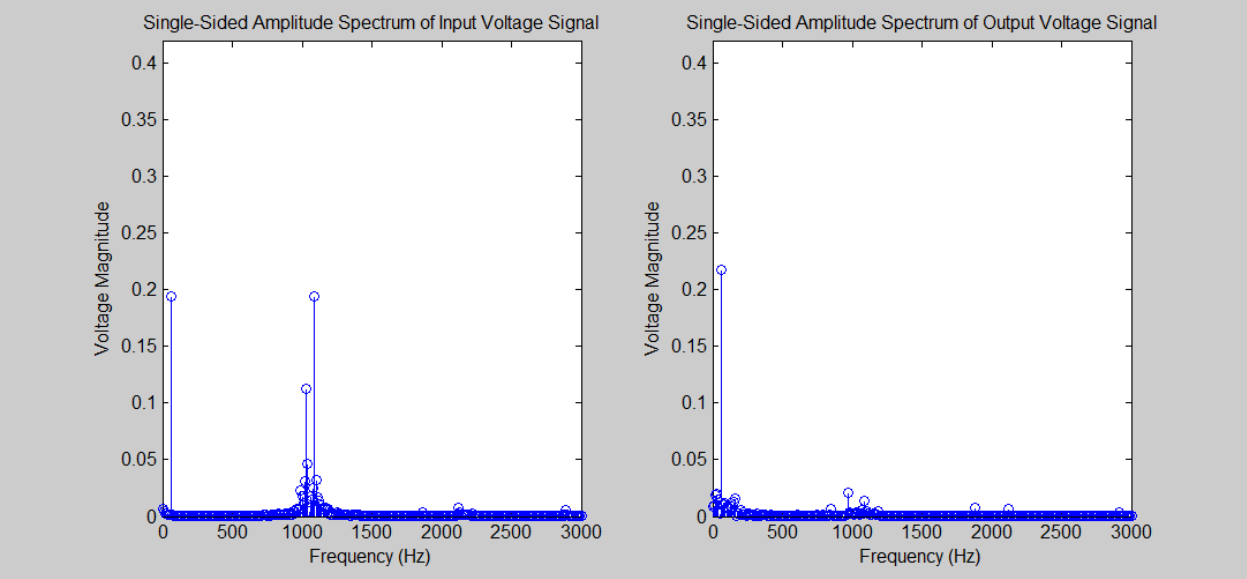


**Figure 5-11.** Fast Fourier Transform of the Input and Output Signal from a Larger Scale of Frequencies

## **6.0 HARMONIC ESTIMATION TECHNIQUES**

This section studies the techniques were used in an attempt to estimate the harmonics of the static Kramer drive signals. Three methods in total are explored.

The first thing that had to be done in order to design a proper filter was to decimate the signals. To get an accurate simulation in SimPowerSystems an adequate sampling time of 2  $\mu$ s was selected, however this led to a signal that contained many data points and had to be decimated.

Since the frequencies that contained the majority of the energy were around the 60 Hz, 1000 Hz and 2000 Hz frequencies a decimated sampling frequency of 5000 Hz was selected. This new frequency satisfies the Nyquist criterion for the 2000 Hz signal so it is an adequate choice.

### **6.1.1 Estimation through the Use of a Band Pass Filter**

The first logical choice to estimate the harmonics of the output wave was the band-pass filter. Since the only frequency that we are interested in is the 60 Hz frequency, theoretically, a filter could be designed so that it only passes the 60 Hz frequency and all of sub-harmonics below 60 Hz and the inter-harmonics and harmonics above 60 Hz are not passed. However, this proved to be more difficult in practice. The band pass filter would be probably be an adequate choice if

the frequencies in the 60 – 360 Hz range were considered, however since the higher frequencies were in the 1000 – 2000 Hz region the band pass filter did not suffice.

### 6.1.1.1 Analytical Development for Band Pass Filter

The analytical development of the band pass filter is derived in this section. As is the case with standard signal processing techniques we will use the input signal whether it be voltage or current denoted by  $x[n]$  in the time domain and  $X[z]$  in the z domain. The output signal will be denoted by  $y[n]$  in the time domain and by  $Y[z]$  in the z domain. Lastly the transfer function or the digital FIR filter will be represented by  $h_b[n]$  in the time domain and  $H_b[z]$  in the z domain.

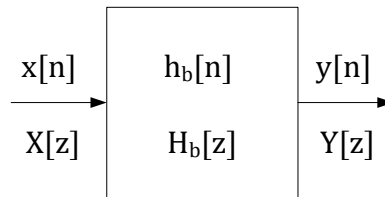


**Figure 6-1.** Block Diagram Representation of the Band Pass Filter

It can be seen from Figure 6-1 that the output is simply the input signal with the proper filtering of the frequencies which are specified in the beginning of this section. A band pass filter would need to cut off the frequencies below and above the 60 Hz fundamental frequency. Therefore taking a proper  $\delta$  which would correctly attenuate the signal would be the goal for the filter to achieve. This  $\delta$  can be seen in the following equation

$$f_c = f_1 \pm \delta \quad (6.1)$$

Choosing one delta makes the band pass filter symmetrical. For this study a symmetrical band pass filter was chosen. Using the  $\delta$  which was described previously the band pass filter's

frequency response equation could be derived. Using a signal length of 500 discrete points gives filter parameters as follows.

$$M = N/2 = 500/2 = 250 \quad (6.2)$$

$$\omega_{c1} = \pi(f_1 - \delta) = \pi\left(\frac{60 - 30}{1000}\right) = 0.0942 \quad (6.3)$$

$$\omega_{c2} = \pi(f_1 + \delta) = \pi\left(\frac{60 + 30}{1000}\right) = 0.2827 \quad (6.4)$$

Using the previously derived parameters the equation for the frequency response of the ideal band pass filter which produces the results described in this section is determined as the following.

$$h_b[n] = \begin{cases} \frac{\sin[0.2827(n - 250)]}{\pi(n - 250)} - \frac{\sin[0.0942(n - 250)]}{\pi(n - 250)} & ; n \neq 250 \\ 0.0600; & n = 250 \end{cases} \quad (6.5)$$

The frequency response of the filter derived above can be seen on a normalized frequency scale in the following figure.

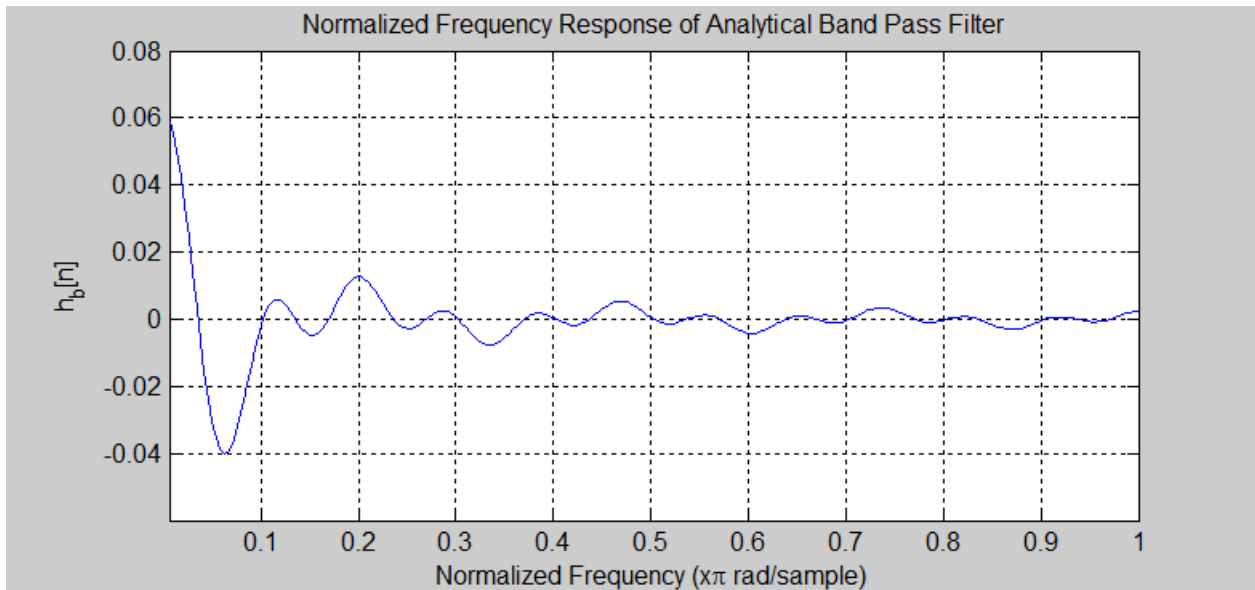


**Figure 6-2.** Frequency Response of Analytic Band Pass Filter

Likewise the magnitude response of the band pass filter can be seen in Figure 6-3. A comparison with the analytic band pass filter and the MATLAB simulated band pass filter will be made at the end of this section.

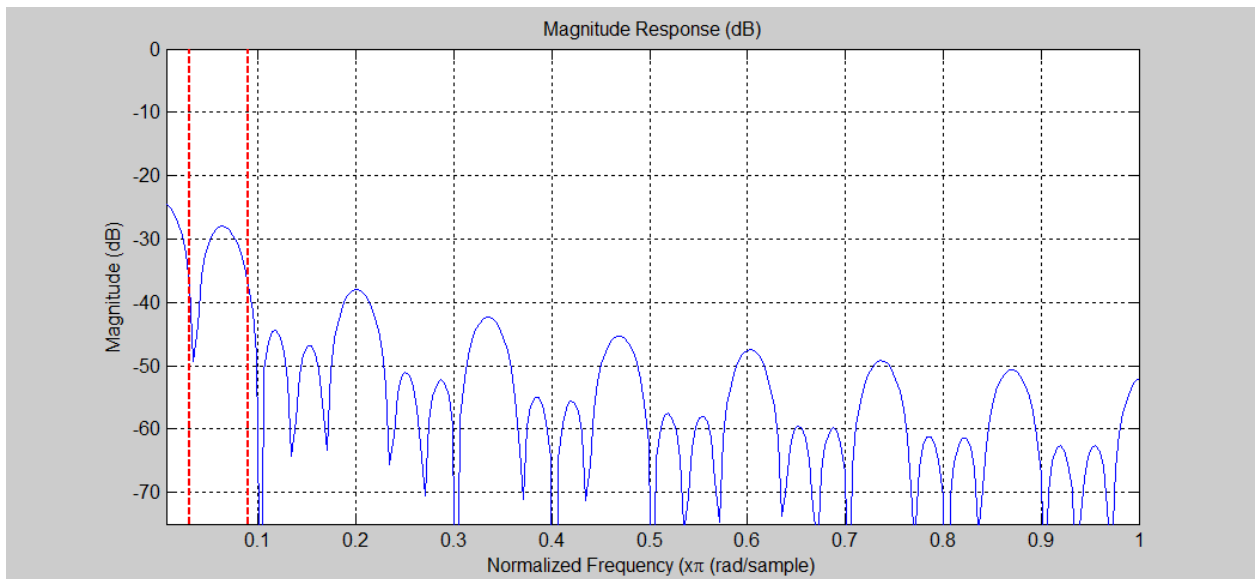


**Figure 6-3.** Magnitude Response of Analytic Band Pass Filter

### 6.1.1.2 Simulation Results of the Band Pass Filter

The filter that was derived in the previous section was implemented using MATLAB. In the ideal situation as was derived in the analytic section only the frequencies from 30-90 Hz would be passed. Figure 6-4 illustrates the normalized frequency response for the MATLAB band pass filter that was used in an effort to filter out the undesirable frequencies.

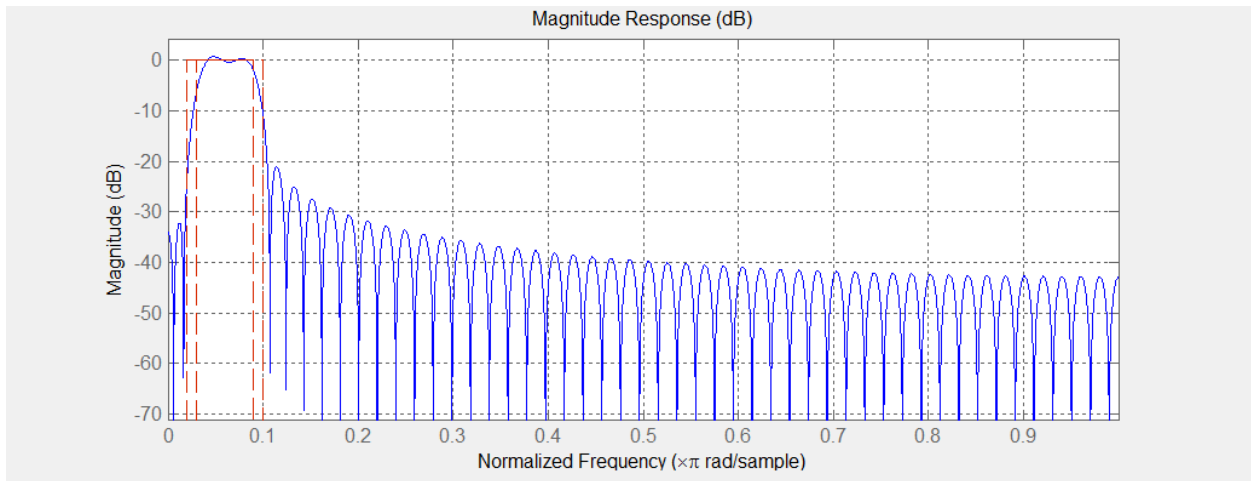


**Figure 6-4.** Frequency response for Least-Squares Band-Pass Filter

It can be seen from this figure that although the undesirable frequencies were filtered out, the bandwidth of the filter was too small to accurately pass the 60 Hz fundamental frequency. It can be seen from Figure 6-5 that the peak to peak output voltage wave has been reduced significantly compared to the original output voltage waveform in Figure 5-9.

It can be seen from Figure 6-5 that signal was cleaned up quite a bit, however there are three problems that exist with this signal. The first problem was that the peak-to-peak value of the voltage was reduced significantly and this voltage is too small to feed back into the system. The second problem is that there is still some noticeable harmonic distortion that remains in the

signal. The third and last problem with the band pass filter is that the output waveform is shifted in phase from the original signal. For the aforementioned reasons the band pass filter was not the optimal filtering choice to clean up the output waveform and feed 60 Hz power back into the system.

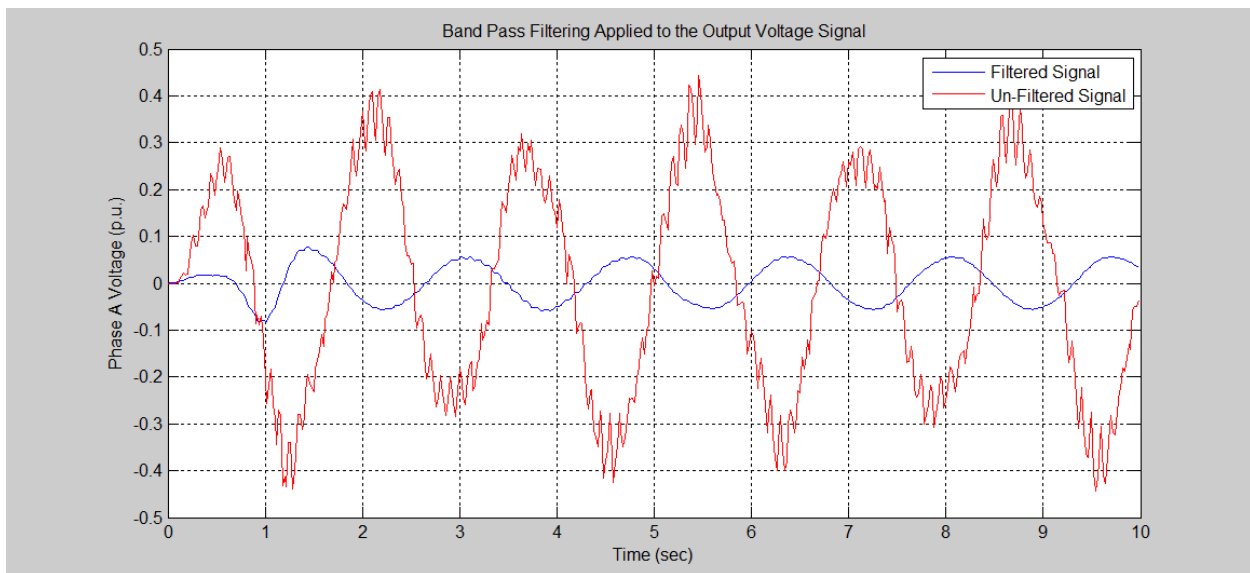


**Figure 6-5.** Voltage Wave with Band Pass Filter Applied

### 6.1.2 Estimation through the Use of a Low Pass Filter

The second choice of a filter to use to clean up the output waveform was a low-pass filter. For this application, both an analytic low pass filter and an equiripple low pass filter were designed using MATLAB which has a pass band of 200 Hz and a stop band of 300 Hz.

### 6.1.2.1 Analytical Development of the Low Pass Filter

The analytical development of the low bass filter is derived in this section. As is the case with standard signal processing techniques we will use the input signal whether it be voltage or current denoted by  $x[n]$  in the time domain and  $X[z]$  is the  $z$  domain. The output signal will be denoted by  $y[n]$  in the time domain and by  $Y[z]$  in the  $z$  domain. Lastly the transfer function or the digital FIR filter will be represented by  $h_b[n]$  in the time domain and  $H_b[z]$  in the  $z$  domain.

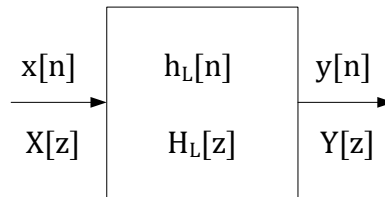


**Figure 6-6.** Block Diagram Representation of the Low Pass Filter

It can be seen from Figure 6-6 that the output is simply the input signal with the proper filtering of the frequencies which are specified in the beginning of this section. A low pass filter would need to cut off the frequencies above the 60 Hz fundamental frequency. Therefore taking a proper  $\delta$  which would correctly attenuate the signal would be the goal for the filter to achieve. This  $\delta$  can be seen in the following equation

$$f_c = f_1 + \delta \quad (6.6)$$

Using the  $\delta$  which was described previously described, the low pass filter's frequency response equation could be derived. Using a signal length of 500 discrete points gives filter parameters as follows.

$$M = N/2 = 500/2 = 250 \quad (6.7)$$

$$\omega_c = \pi(f_1 + \delta) = \pi\left(\frac{200}{1000}\right) = 0.6283 \quad (6.8)$$

Using the previously derived parameters the equation for the frequency response of the ideal band pass filter which produces the results described in this section is determined as the following.

$$h_L[n] = \begin{cases} \frac{\sin[0.6283(n - 250)]}{\pi(n - 250)} & ; n \neq 250 \\ 0.200 & ; n = 250 \end{cases} \quad (6.9)$$

The frequency response of the filter derived above can be seen on a normalized frequency scale in the following figure.

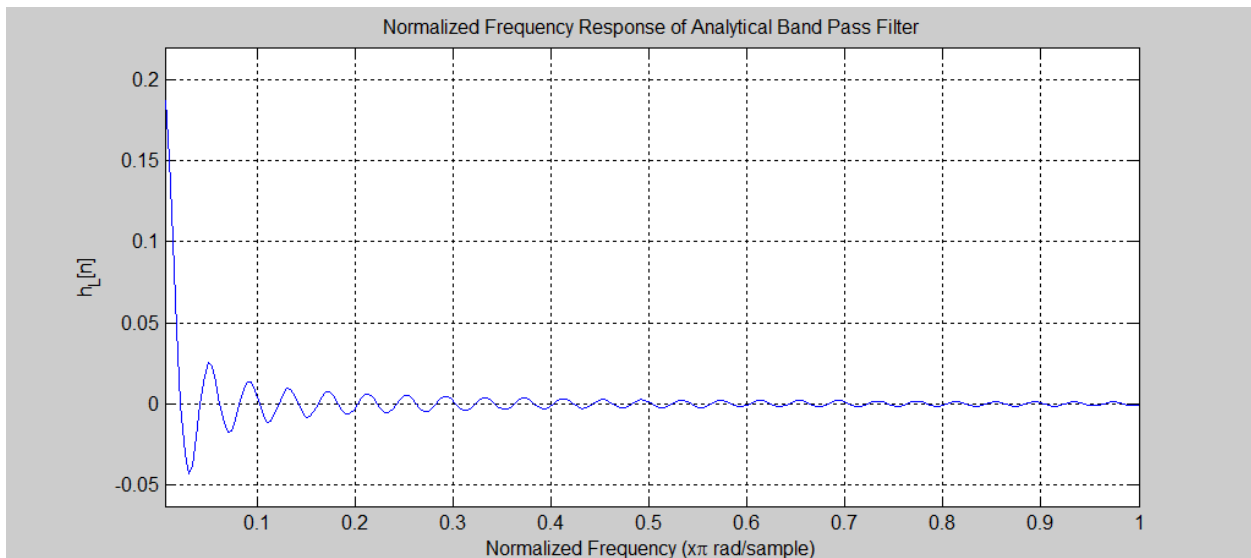


**Figure 6-7.** Frequency Response of Analytic Low Pass Filter

Likewise the magnitude response of the band pass filter can be seen in Figure 6-3. A comparison with the analytic band pass filter and the MATLAB simulated band pass filter will be made at the end of this section.

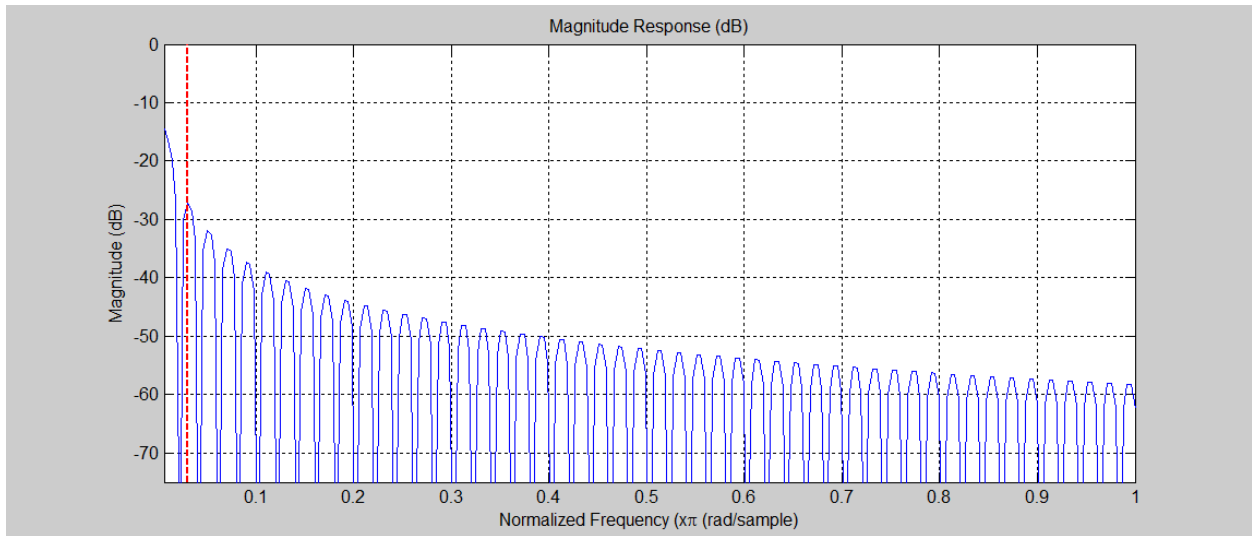


**Figure 6-8.** Magnitude Response of Analytic Low Pass Filter

### 6.1.2.2 Simulation Result of the Low Pass Filter

The frequency response for this filter can be seen in Figure 6-9. Subsequently the filtered output waveform for the low pass filter is shown in Figure 6-10. It can be seen from this figure that the low pass filter is a great improvement from the band pass filter in the sense that the peak-to-peak voltage remained intact. Also, it can be seen from this figure that there is less harmonic distortion than there was with the band pass filter. The problem with the method of low pass filtering alone was also a problem that was seen with the band pass filter. That problem was that the filtered waveform is shifted in phase from the original waveform. To solve this problem an additional filtering technique must be applied.

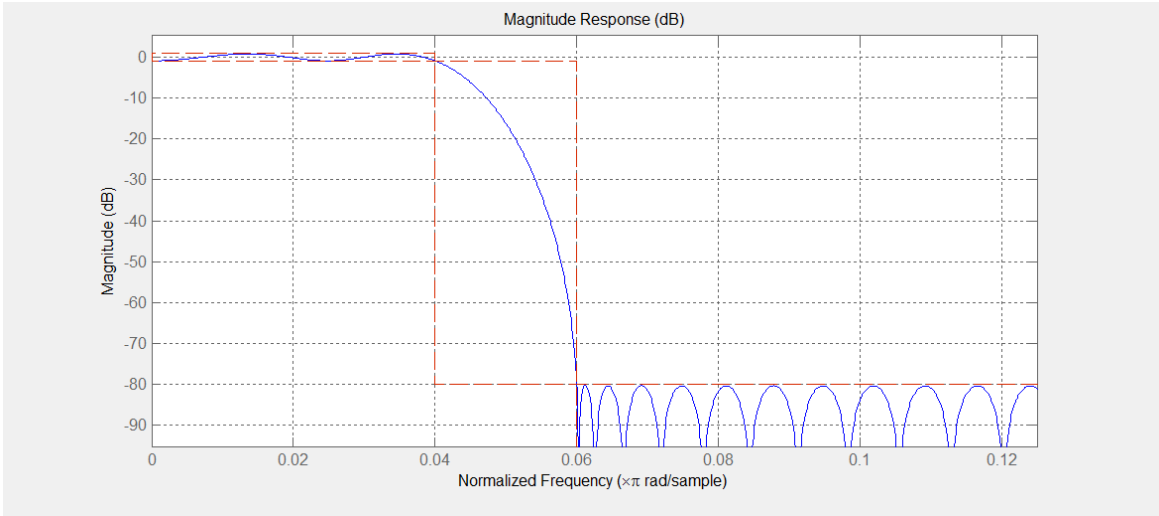


**Figure 6-9.** Frequency Response for Low Pass Equiripple Filter

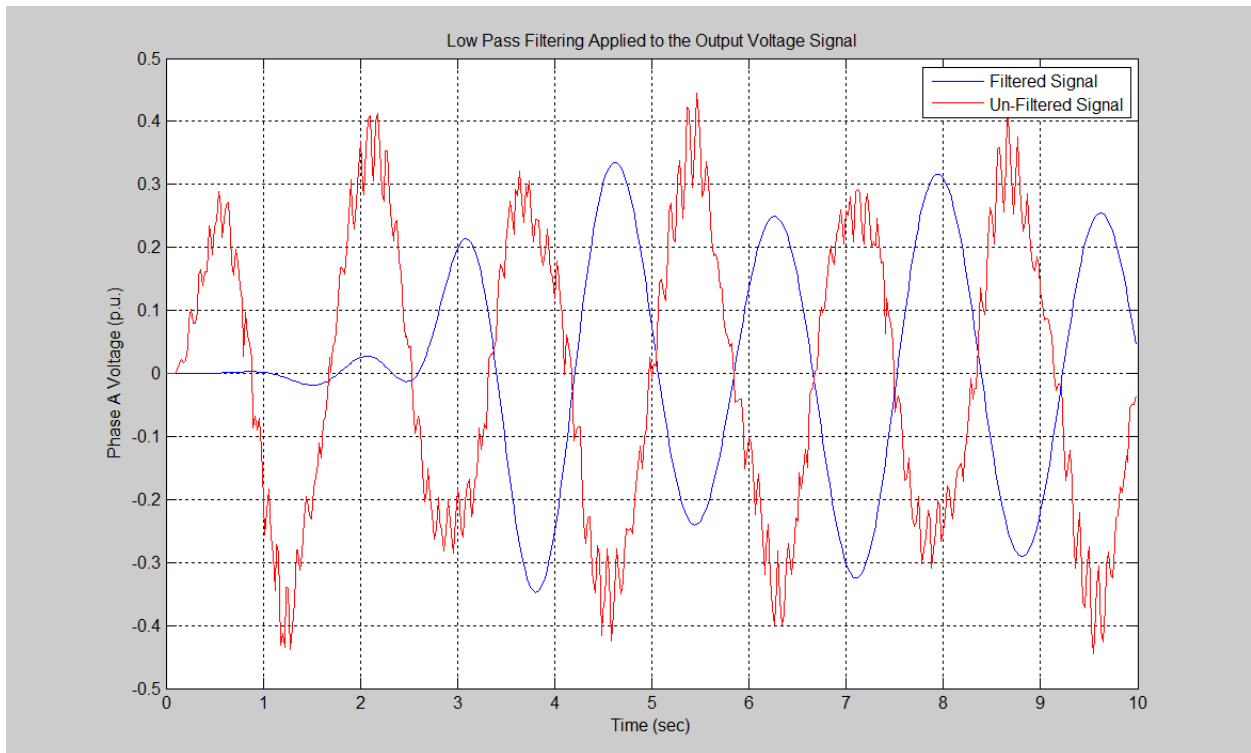


**Figure 6-10.** Voltage Wave with Low Pass Filter Applied

### 6.1.3 Estimation through the a Phase Shifting Low Pass Filter

The same lower pass filter that was used in the previous section cascaded with an all pass filter. The purpose of the all pass filter is to simply shift the wave form so that it is in phase with the original signal.

#### 6.1.3.1 Analytical Development of the Phase Shifting Low Pass Filter

The analytical development of the phase shifting low pass filter is derived in this section. As is the case with standard signal processing techniques we will use the input signal whether it be voltage or current denoted by  $x[n]$  in the time domain and  $X[z]$  is the  $z$  domain. The output signal will be denoted by  $y[n]$  in the time domain and by  $Y[z]$  in the  $z$  domain. Lastly the transfer function or the digital FIR filter will be represented by  $h_b[n]$  in the time domain and  $H_b[z]$  in the  $z$  domain.

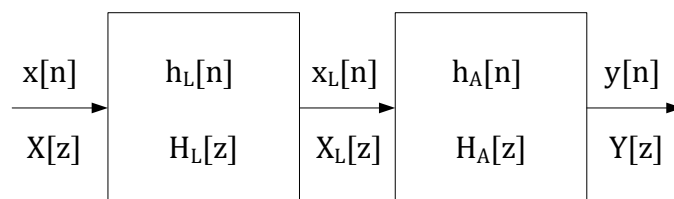


**Figure 6-11.** Block Diagram Representation of the Phase Shifting Low Pass Filter

In order to derive the phase shifting low pass filter it is useful to derive both the low pass and the all pass filter in terms of the frequency response and their phase response in order to properly see how the filters work. The following equation shows the Laplace transform of a low pass filter.

$$H_L(s) = \frac{1}{1 + \alpha s} \quad (6.10)$$

where  $\alpha$  is a constant which determines the cutoff frequency of the filter. Taking the frequency response of the low pass filter we have.

$$H_L(j\omega) = \frac{1}{1 + j\alpha\omega} \quad (6.11)$$

Equation 6.11 will give both the magnitude and phase of the low pass filter with varying frequency. The magnitude response of the filter is given by equation 6.12.

$$|H_L(j\omega)| = \frac{1}{\sqrt{1 + (\alpha\omega)^2}} = \frac{1}{\sqrt{1 + \alpha^2\omega^2}} \quad (6.12)$$

It can be seen from this equation that as the frequency  $\omega$  increases the magnitude of the filter subsequently decreases. This is how the filter is expected to operate. In a similar fashion the phase response of the low pass filter is derived in equation 6.13.

$$\angle H_L(j\omega) = \tan^{-1}\left(\frac{0}{1}\right) - \tan^{-1}\left(\frac{1}{\alpha\omega}\right) = -\tan^{-1}\left(\frac{1}{\alpha\omega}\right) \quad (6.13)$$

It can be seen by this equation where the problem arises when using a low pass filter. With the increasing of the frequency the closer the phase is to zero and hence the largest phase shift is at low frequencies. The fundamental frequency in this case is considered a low frequency and hence there is a significant shift in phase.

Next the all pass filter will be derived in this Laplace domain. The following equation shows the equation for the Laplace transform of an all pass filter.

$$H_A(s) = \frac{\beta s - 1}{\beta s + 1} \quad (6.14)$$

where  $\beta$  is a constant which determines the phase shift of the filter. Taking the frequency response of the all pass filter we have.

$$|H_A(j\omega)| = \frac{\sqrt{(\beta\omega)^2 + (-1)^2}}{\sqrt{(\beta\omega)^2 + (1)^2}} = 1 \quad (6.15)$$

It can be seen from equation 6.14 that the filter passes all frequencies which is the expected result. In a similar fashion the phase response of the low pass filter is derived in equation 6.15.

$$\angle H_A(j\omega) = \tan^{-1}\left(\frac{\beta\omega}{-1}\right) - \tan^{-1}\left(\frac{\beta\omega}{1}\right) = \pi - 2 \tan^{-1}(\beta\omega) \quad (6.16)$$

Equation 6.15 shows that for a frequency of zero, the phase shift of the filter is equal to 180 degrees decreases with increasing frequency. The limit of the filters phase shift as the frequency approaches infinity is zero phase shift. The constant  $\beta$  dictates the amount that the signal is shifted for a given frequency.

Then to derive the phase shifting low pass filter's time domain function there are two options. The first option is to take the convolution of the two filters as is shown in equation 6.17.

$$h_{ps}(t) = h_L(t) * h_A(t) = \int_0^t h_L(t-\tau)h_A(\tau)d\tau \quad (6.17)$$

However, a much easier approach to deriving the transfer function for the phase shifting low pass filter's time domain function is to multiply the transfer function of each of the filters in the Laplace domain, decompose them with partial fraction decomposition and then take the inverse Laplace transform yielding the time domain equation. This is shown in the following derivation.

$$H_{ps}(s) = H_L(s)H_A(s) = \frac{\beta s - 1}{\beta s + 1} \frac{1}{\alpha s + 1} = \frac{\beta s - 1}{(\beta s + 1)(\alpha s + 1)} \quad (6.18)$$

Then decomposing the function into partial fractions we have

$$\frac{\beta s - 1}{(\beta s + 1)(\alpha s + 1)} = \frac{A}{(\alpha s + 1)} + \frac{B}{(\beta s + 1)} \quad (6.18)$$

$$(\beta s - 1) = A(\beta s + 1) + B(\alpha s + 1) \quad (6.19)$$

$$\beta s - 1 = (A\beta + B\alpha)s + (A + B) \quad (6.20)$$

This can then be transformed to the matrix system shown in equation 6.21

$$\begin{bmatrix} \beta & \alpha \\ 1 & 1 \end{bmatrix} \begin{bmatrix} A \\ B \end{bmatrix} = \begin{bmatrix} \beta \\ -1 \end{bmatrix} \quad (6.21)$$

Solving the system in equation 6.21 yields the solution in equation 6.22.

$$H_{ps}(s) = \frac{-1}{(\alpha - \beta)(\alpha s + 1)} + \frac{2\beta}{(\alpha - \beta)(\beta s + 1)} \quad (6.22)$$

Taking the inverse Laplace transform of equation 6.22 yields the time domain solution for the phase shifting transform.

$$h_{ps}(t) = \frac{-1}{(\alpha - \beta)} e^{-\alpha t} + \frac{2\beta}{(\alpha - \beta)} e^{-\beta t} \quad (6.23)$$

### 6.1.3.2 Analysis of the Phase Shifting Low Pass Filter's Tuning Parameters

The zero crossing of the input signal  $x[n]$  can then be used to properly tune the parameters  $\alpha$  and  $\beta$  so that the filter both attenuates the proper frequencies and shifts the phase in a manner such that original signal and the estimated signal are in phase. The result of this can be seen in the following section.

As was previously stated the tuning parameters  $\alpha$  and  $\beta$  can be varied to achieve the desired attenuation and phase shift of the filter. The effects of varying these tuning parameters were shown using MATLAB. Figure 6-11 and Figure 6-12 illustrate the effect of varying the  $\alpha$  parameter with respect to the filter's magnitude frequency response and phase

frequency response respectively. It can be seen from these figures that both the magnitude and phase response are quite versatile and can achieve the desired attenuation, which in turn results in a shift in phase.

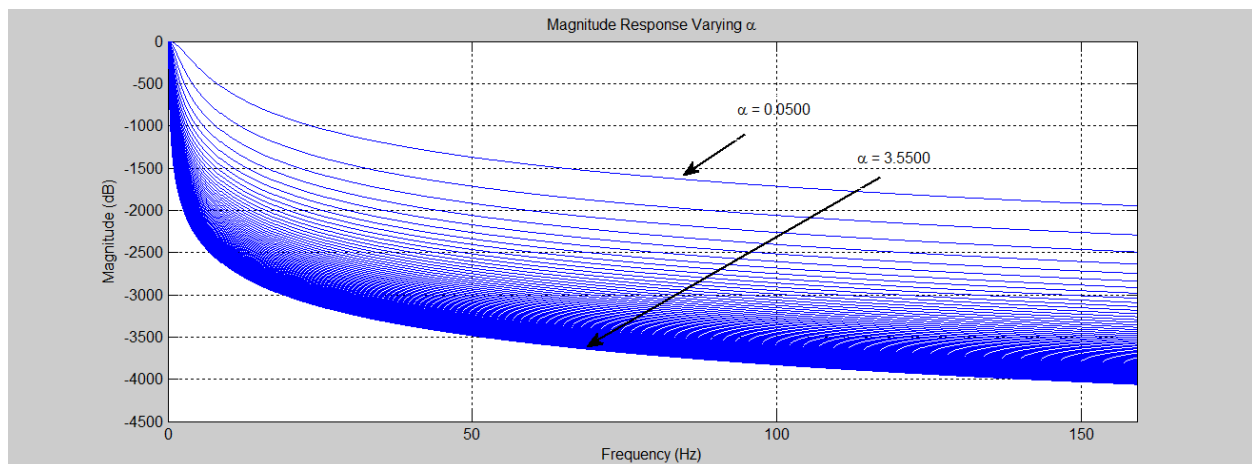


**Figure 6-12.** Magnitude Response of Phase Shifting Low Pass Filter with Respect to Varying  $\alpha$

The benefit of the phase shifting low pass filter is that one can effectively attenuate a signal passing the desired frequencies like in the case of the low pass filter but there is also one extra tuning parameter  $\beta$  which can be used to shift the phase to the desired value. Therefore the correct method of using the phase shifting low pass filter is to choose a value of the tuning parameter  $\alpha$  such that the signal is properly attenuated and then use the  $\beta$  tuning parameter to correct any phase shift produced by the low pass filter component.

The effectiveness of the  $\beta$  tuning parameter with respect to phase shift can be seen in Figure 6-13. It can be seen from this figure that one could produce the desired phase shift for a given frequency easily by varying the value of  $\beta$ .

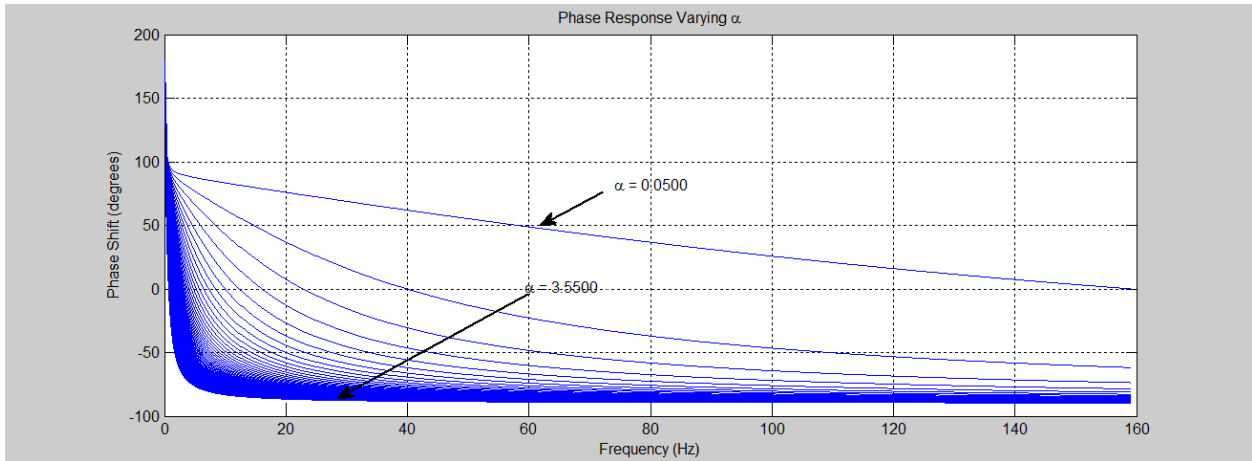


**Figure 6-13.** Phase Response of Phase Shifting Low Pass Filter with Respect to Varying  $\alpha$

This should be very apparent especially for the smaller frequencies that would be produced from a power system.

It should be noted that the magnitude response for a varying value of the tuning parameter  $\beta$  does not need to be analyzed due to the fact that this parameter arises from the all pass filter.

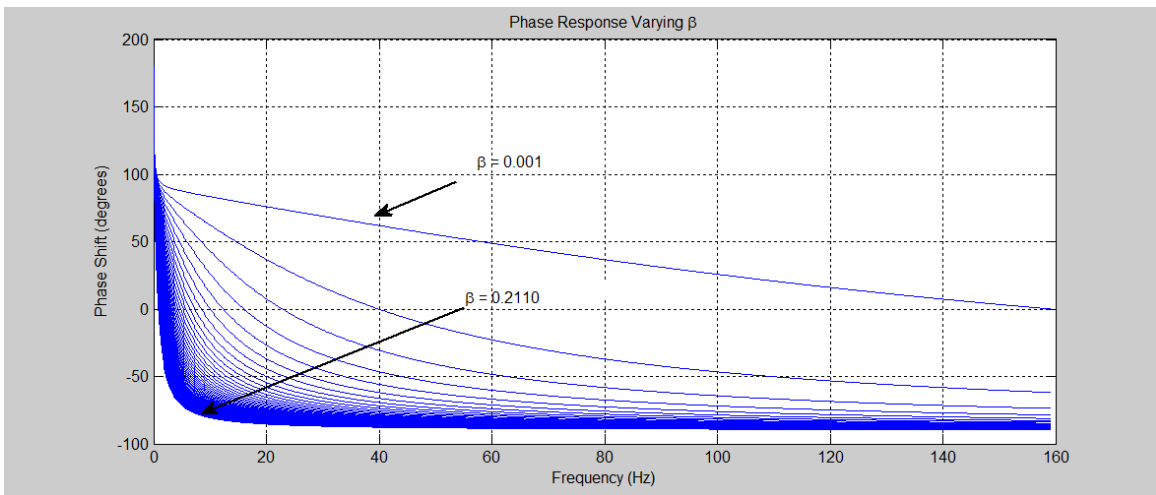


**Figure 6-14:** Phase Response of Phase Shifting Low Pass Filter with Respect to Varying  $\beta$

It was previously shown in equation 6.15 that the all pass filter has a magnitude response of 0 dB for all operating frequencies. For this reason the magnitude response as a function of the  $\beta$  parameter is omitted.

The phase shifting low pass filter was used with the zero crossing computation from the low pass filter implementation showed that the output signal from the low pass filter was approximately 200 degrees or 3.49 rads out of phase with the original signal. Solving for the  $\beta$  parameter is shown in the following set of equations.

$$\pi - 2 \tan^{-1}(\beta\omega) = 3.49 \quad (6.24)$$

$$\beta = \frac{\tan(0.1745)}{0.6283} = 0.2806 \quad (6.25)$$

Then solving for the  $\alpha$  parameter is shown in the following equation.

$$\alpha = \frac{1}{\omega_c} = \frac{1}{0.6283} = 1.5916 \quad (6.26)$$

This yields the numeric time domain solution to the phase shifting low pass filter given in the following equation

$$h_{ps}(t) = -0.7628e^{-1.5916t} + 0.4281e^{-0.2806t} \quad (6.27)$$

### 6.1.3.3 Simulation of the Phase Shifting Low Pass Filter

The phase shifting low pass filter that was derived in the previous equation was simulated using MATLAB. The results of the simulation are shown in this section. The original signal is plotted versus the clean estimated signal in Figure 6-14. It can be seen from this new signal that the method described in this section was quite efficient in estimating a clean 60 Hz signal which was in phase with the original signal.

The resulting Fourier analysis plot is shown in Figure 6-15. It can be seen from this figure that the vast majority of the energy is focused in the 60 Hz frequency as desired. All of the

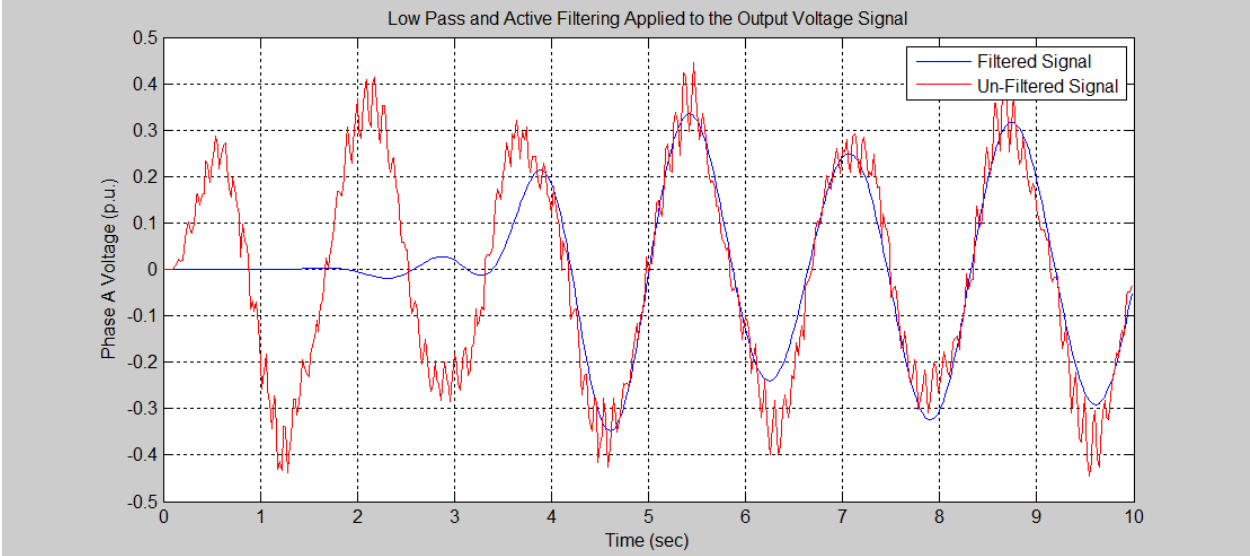


**Figure 6-15.** Voltage Wave with Low Pass and All Pass Filter Applied

energy that existed in around the 1000 and 2000 Hz frequencies was eliminated by the filtering techniques applied. There is still a small amount of energy in the sub-harmonic and interharmonics frequencies that surround the 60 Hz frequency but the total harmonic distortion was significantly reduced from the original signal that was being fed back into the original system.

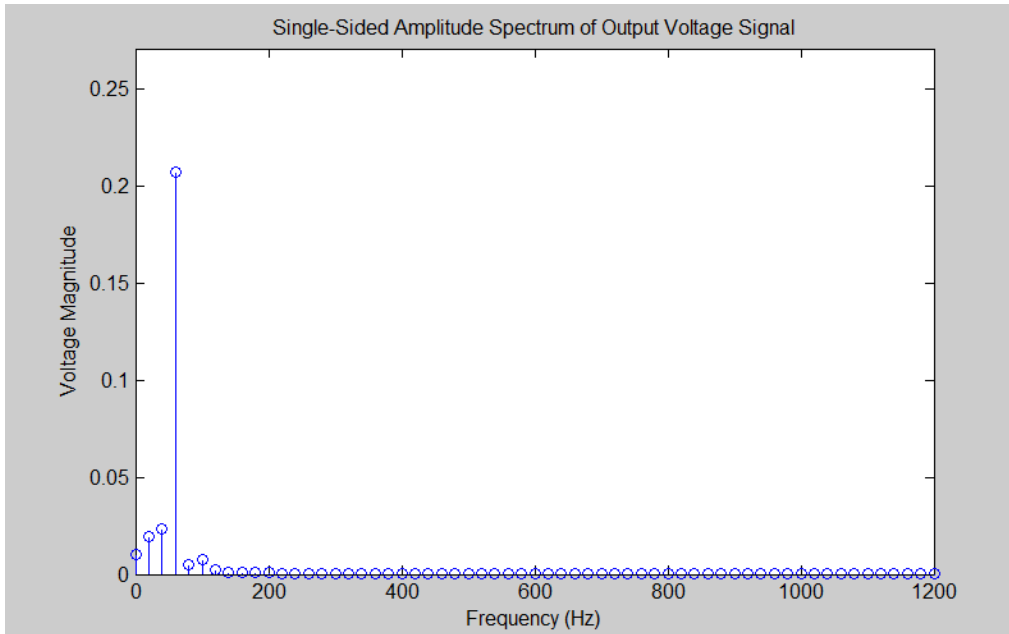


**Figure 6-16.** Fourier Analysis for the Low Pass and All Pass Filtered Signal

There are further techniques that may be applied to try and clean up the signal even more and reduce the overall harmonic distortion such as active filtering by means of current injection at these sub-harmonic and interharmonic frequencies but these methods may provide too costly for the little benefit that they may provide.

## 7.0 DISCUSSION

The static Kramer drive system was chosen to be the main focus test system for this doctoral thesis. However, this work is not only intended to be for the static Kramer drive system. The goal here is to develop the methodology to eliminate interharmonics and sub-harmonics while still doing an effective job of eliminating classical harmonics. Therefore the methods that are used here will be a platform to solutions to other systems. Many motor drive systems will be very similar to the static Kramer drive system and some of the techniques that will be developed will be applicable without making any alterations. However, some systems may be quite a bit different but the techniques developed in this work will still be effective after some kind of alteration. It is with this in mind that the techniques will be developed and therefore there will be some “hooks” left into the development so that these alterations can be made easily without having to alter too much.

## 8.0 CONCLUSION

The focus of this study was to apply signal processing techniques of estimation to the Static Kramer Drive system in order to adequately estimate classic harmonics, interharmonics and sub-harmonics to aid the power industry in the eventual elimination of costly harmonic distortion.

It is evident that with the ever changing power system grid that new challenges due to harmonic distortion will continue to be a factor as long as there are new advances in power electronic technology. One of the most effective ways to eliminate harmonics in power systems today are through adequate means of estimation especially when considering the lesser studied interharmonics and sub-harmonics.

A great deal of information which is essential for the estimation of harmonics in power system is determined by Fourier analysis of a system broken down and likewise as a whole. In this study the major components which produced harmonic distortion was determined by breaking the system down and performing Fourier analysis on the system. It was shown that this analysis could be used as the building blocks for classic techniques of signal processing estimation such as digital filtering and likewise for more advanced techniques such digital filter tuning to provide optimal estimation. The methods that were used in this study such as phase shifting digital low pass filtering were shown to be quite superior to those of the more classical techniques such as simple low pass and simple band pass filtering.

This study can be used to develop further research topics which fall into the same category. The main focus presented was the estimation of harmonics in motor drive systems. Simply estimating harmonic signals provides a great deal of useful information about damaging voltage and current signals in a system but the overall solution to maintain a nearly harmonic free system is to couple the methods of estimation shown in this study with methods of harmonic elimination which were discussed in the literature review of this paper.

Work that can be done in the near future which will further the developments stated in this paper is the coupling of the developed estimation techniques with signal processing measurement techniques and active filtering to ultimately remove the harmonic distortion from the system.

Furthermore it is known that methods of estimation, measurement and active filtering are all a solution but come at a cost. A cost analysis would determine if an overall estimation/elimination solution would indeed provide a cost effective solution and in turn determine if an adequate return on investment would be achieved.

It is apparent from this study that the Static Kramer Drive System is just one of many systems that exist in power systems today which generate harmonic distortion. Ultimately it would be a worthy experiment to compare the methods that were used for the Static Kramer Drive System on other motor drive systems to compare the effectiveness of the methods. It would also be useful to compare these methods to systems that exist in power systems which generate harmonics but are not motor drive systems such as arc furnace systems and data center systems.

## BIBLIOGRAPHY

1. Arrillaga, J. and N.R. Watson, *Power system harmonics*. 2nd ed2003, West Sussex, England ; Hoboken, NJ: J. Wiley & Sons. x, 399 p.
2. Ray, P.K. and B. Subudhi, *Ensemble-Kalman-Filter-Based Power System Harmonic Estimation*. Instrumentation and Measurement, IEEE Transactions on, 2012. **PP**(99): p. 1-9.
3. *Interharmonics in Power Systems - IEEE Interharmonic Task Force, Cigré 36.05/CIREN 2 CC02 Voltage Quality Working Group*.
4. *IEEE Recommended Practices and Requirements for Harmonic Control in Electrical Power Systems*. IEEE Std 519-1992, 1993: p. 0\_1.
5. De Abreu, J.P.G. and A.E. Emanuel. *The need to limit subharmonics injection*. in *Harmonics and Quality of Power, 2000. Proceedings. Ninth International Conference on*. 2000.
6. Al Zahawi, B.A.T., B.L. Jones, and W. Drury, *Analysis and simulation of static Kramer drive under steady-state conditions*. Electric Power Applications, IEE Proceedings B, 1989. **136**(6): p. 281-292.
7. Kushare, B.E., A.A. Ghatol, and M.S. Aphale. *Survey of interharmonics in Indian power system network*. in *Power Engineering Conference, 2007. IPEC 2007. International*. 2007.
8. LLC, E.S. *Harmonics*. 2005; Available from: <http://www.touchstoneenergy.com/efficiency/bea/Documents/Harmonics.pdf>.
9. Sang-Wook, S., et al., *A Filter Bank and a Self-Tuning Adaptive Filter for the Harmonic and Interharmonic Estimation in Power Signals*. Instrumentation and Measurement, IEEE Transactions on, 2012. **61**(1): p. 64-73.
10. Fourier, J.B.J., *Theorie Analytique de la Chaleur*1822, Paris, France.
11. Chaparro, L.F., *Signals and Systems Using MATLAB*. 1 ed2010.
12. Oppenheim, A.V. and A.S. Willsky, *Signals & Systems*. 2 ed1996.
13. Glover, J.D., M.S. Sarma, and T.J. Overbye, *Power system analysis and design*. 4th ed2008, Australia ; Toronto, Ont.: Thomson. xvi, 752 p.
14. Grainger, J.J. and W.D. Stevenson, *Power system analysis*. McGraw-Hill series in electrical and computer engineering Power and energy1994, New York: McGraw-Hill. xix, 787 p.

15. Fuchs, E.F., D.J. Roesler, and M.A.S. Masoum, *Are harmonic recommendations according to IEEE and IEC too restrictive?* Power Delivery, IEEE Transactions on, 2004. **19**(4): p. 1775-1786.
16. 1000-2-1, C.I., *Electromagnetic Compatibility*, in *Description of the Environment - Electromagnetic environment for low-frequency conducted disturbances and signalling in public power supply systems*1990.
17. Yacamini, R., *Power system harmonics. IV. Interharmonics*. Power Engineering Journal, 1996. **10**(4): p. 185-193.
18. Chu, R.F. and J.J. Burns, *Impact of cycloconverter harmonics*. Industry Applications, IEEE Transactions on, 1989. **25**(3): p. 427-435.
19. Pelly, B.R., *Thyristor Phase-Controlled Converters and Cycloconverters* 1971, New York, NY: John Wiley and Sons.
20. Leonowicz, Z. *Analysis of sub-harmonics in power systems*. in *Environment and Electrical Engineering (EEEIC), 2010 9th International Conference on*. 2010.
21. Rahimi, A.M., A. Khalilgh, and A. Emadi. *Sub-Harmonic Problem in Multi-Converter Vehicular Power Systems*. in *Vehicle Power and Propulsion Conference, 2006. VPPC '06. IEEE*. 2006.
22. Harlow, J.H., *Electric Power Transformer Engineering*2004: CRC Press.
23. McNames, J., *Second Order Filters Overview*, Portland State University.
24. Izhar, M., et al. *Performance for passive and active power filter in reducing harmonics in the distribution system*. in *Power and Energy Conference, 2004. PECon 2004. Proceedings. National*. 2004.
25. Sasaki, H. and T. Machida, *A New Method to Eliminate AC Harmonic Currents by Magnetic Flux Compensation-Considerations on Basic Design*. Power Apparatus and Systems, IEEE Transactions on, 1971. **PAS-90**(5): p. 2009-2019.
26. Fang Zheng, P., *Application issues of active power filters*. Industry Applications Magazine, IEEE, 1998. **4**(5): p. 21-30.
27. Round, S., *Active Filtering and VAR Compensation*, 1992, University of Canterbury: New Zealand.
28. Stengel, R.F., *Optimal control and estimation*. Dover books on advanced mathematics1994, New York: Dover Publications. xvi, 639 p.
29. Chen, C.-T., *Linear system theory and design*. 3rd ed. The Oxford series in electrical and computer engineering1999, New York: Oxford University Press. xiii, 334 p.

30. Gelb, A. and A.S.C.T. Staff., *Applied optimal estimation* 1974, Cambridge, Mass.,: M.I.T. Press. 374 p.
31. Gauss, C.F. and C.H. Davis, *Theory of the motion of the heavenly bodies moving about the sun in conic sections* 1963, New York,: Dover Publications. xvii, 326 p., 39 p. of tables.
32. Sorenson, H.W., *Least-Square Estimation: From Gauss to Kalman*, IEEE Spectrum, 1970. **July 1970**.
33. Everitt, B. and D.C. Howell, *Encyclopedia of statistics in behavioral science* 2005, Hoboken, N.J.: John Wiley & Sons.
34. Hongbin, L., P. Stoica, and L. Jian. *Parameter estimation for harmonic sinusoidal signals*. in *Signals, Systems, and Computers, 1999. Conference Record of the Thirty-Third Asilomar Conference on*. 1999.
35. Bose, B.K., *Modern power electronics and AC drives* 2002, Upper Saddle River, NJ: Prentice Hall. xxi, 711 p.
36. Testa, A., D. Gallo, and R. Langella, *On the Processing of harmonics and interharmonics: using Hanning window in standard framework*. Power Delivery, IEEE Transactions on, 2004. **19**(1): p. 28-34.
37. wikipedia.com. *Window Function*. Available from: [http://en.wikipedia.org/wiki/Window\\_function](http://en.wikipedia.org/wiki/Window_function).
38. Chapman, S.J., *Electric machinery fundamentals*. 4th ed 2005, New York, NY: McGraw-Hill Higher Education. xxii, 746 p.
39. Company, B.E. *Severe Duty Motors*. [Datasheet]; Available from: <http://www.baldor.com/support/Literature/Load.ashx/BR420?LitNumber=BR420>
40. Circuits, A.A. *Rectifier Circuits*. 2003-2012; Available from: [http://www.google.com/imgres?q=three+phase+rectifier+current+waveform&um=1&hl=en&safe=off&sa=X&tbo=d&biw=1366&bih=643&tbm=isch&tbnid=6iYJI9KxkwviM:&imgrefurl=http://www.allaboutcircuits.com/vol\\_3/chpt\\_3/4.html&docid=qulj63SHFUWpwM&imgurl=http://sub.allaboutcircuits.com/images/03269.png&w=545&h=232&ei=f16iUMTJIKPn0gGir4CwBA&zoom=1&iact=hc&vpx=629&vpy=374&dur=1175&hovh=146&hovw=344&tx=201&ty=98&sig=106791703616831200879&page=2&tbnh=112&tbnw=256&start=21&ndsp=28&ved=1t:429,r:19,s:20,i:191](http://www.google.com/imgres?q=three+phase+rectifier+current+waveform&um=1&hl=en&safe=off&sa=X&tbo=d&biw=1366&bih=643&tbm=isch&tbnid=6iYJI9KxkwviM:&imgrefurl=http://www.allaboutcircuits.com/vol_3/chpt_3/4.html&docid=qulj63SHFUWpwM&imgurl=http://sub.allaboutcircuits.com/images/03269.png&w=545&h=232&ei=f16iUMTJIKPn0gGir4CwBA&zoom=1&iact=hc&vpx=629&vpy=374&dur=1175&hovh=146&hovw=344&tx=201&ty=98&sig=106791703616831200879&page=2&tbnh=112&tbnw=256&start=21&ndsp=28&ved=1t:429,r:19,s:20,i:191).
41. Three-Phase AC-DC-AC PWM Conveter, Available from <http://www.mathworks.com/matlabcentral/fileexchange/34272-three-phase-ac-dc-ac-pwm-converter>